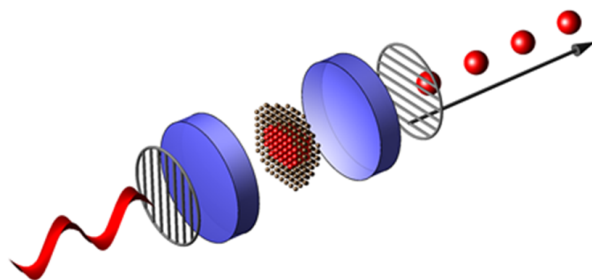




---

# Optimizing the polarization for a brighter CQED Single Photon Source

---



THESIS

submitted in partial fulfillment of the  
requirements for the degree of

MASTER OF SCIENCE

in

PHYSICS

Author :	M.F. van de Stolpe
Student ID :	s0000000
Supervisor :	MSc. H.J. Snijders Dr. W. Löffler
	Prof.dr. D. Bouwmeester
2 <sup>nd</sup> corrector :	Prof.dr. M.P. van Exter

Leiden, The Netherlands, April 13, 2017



# Optimizing the polarization for a brighter CQED Single Photon Source

**M.F. van de Stolpe**

Huygens-Kamerlingh Onnes Laboratory, Leiden University  
P.O. Box 9500, 2300 RA Leiden, The Netherlands

April 13, 2017

## **Abstract**

Self-assembled InAs/GaAs quantum dots currently have the highest overall single photon source (SPS) performance, but one of the limiting factors for the brightness is the extraction of single photons from the excitation laser pulse. Since the SPS is excited resonantly for maximal indistinguishability, a difference in polarization is used to extract the single photons from the incident excitation laser light. In this work we studied ways to maximize the collection of single photons and the brightness of the SPS both experimentally and theoretically. The system of a quantum dot in an optical cavity was simulated semi classically. Two new brighter configurations for the input and output polarization were found, one through analytical analysis and one with an optimization algorithm. These two new polarization configurations were tested in the lab along with the configuration that is conventionally used, which resulted in an SPS which was *twice* (analytical analysis) and *three* times (optimization algorithm) as bright as the conventional configuration. We show that the brightness can be improved by another factor of three through optimizing one of the sample dependent parameters determined in sample fabrication.



# Contents

<b>1</b>	<b>Introduction</b>	<b>1</b>
<b>2</b>	<b>Theory and simulation</b>	<b>7</b>
2.1	Semi-classical model	7
2.1.1	Formula	8
2.1.2	Limits	9
2.2	Parameters	9
2.3	Understanding the model	12
2.3.1	Quantum dot angle near $0^\circ$ or $90^\circ$	12
2.3.2	Cavity mode splitting	15
2.4	Optimal polarization configuration	17
2.4.1	Polarization (lab adjustable parameter)	18
2.4.2	Sample dependent parameters	22
<b>3</b>	<b>Materials and Methods</b>	<b>25</b>
3.1	Materials	25
3.1.1	Experimental setup	25
3.1.2	Sample	26
3.2	Methods	27
3.2.1	Laser scan	27
3.2.2	Polarization scan	27
3.2.3	Voltage scan	28
3.2.4	$g^{(2)}(\tau)$ -measurement	28
<b>4</b>	<b>Experimental results and discussion</b>	<b>29</b>
4.1	Sample dependent parameters	30
4.2	Laser scan line shapes	33
4.3	Single photon source quality	36

4.3.1	Single photons and brightness	36
4.3.2	Comparison	40
4.4	Mechanism behind brighter SPS	41
4.5	Discussion on the higher intensity	42
<b>5</b>	<b>Conclusion</b>	<b>47</b>
<b>6</b>	<b>Outlook</b>	<b>49</b>
<b>7</b>	<b>Acknowledgements</b>	<b>51</b>

# Introduction

The discovery of stimulated emission opened a whole new field of research culminating in a set of light sources with high performance, high reliability, yet low cost. These light sources (e.g. LASERs, LEDs) are now used for a broad range of applications in everyday life. The next step in this field of research will be to produce non-classical light sources. These sources are characterized by the ability to control their quantum fluctuations for which a single photon source serves as a major building block [1]. Moreover, these single photon sources are needed for most quantum information technologies [2–7] such as quantum key distribution [8, 9] or boson sampling [10].

Although there is still no ideal single photon source, a host of material systems has been researched for its ability to produce single photons on demand [1] and some of the more promising systems have been engineered to come close to the ideal single photon source. The question this might raise is therefore what such an ideal single photon source looks like.

Aharonovich, Englund and Toth [1] describe the ideal single photon source as follows: “The ideal on-demand SPE (single photon emitter) emits exactly one photon at a time into a given spatiotemporal mode (high purity), and all photons are identical so that if any two are sent through separate arms of a beam-splitter, they produce full interference (a signature of indistinguishability).” But the demands on the source are even higher as for most applications the ideal single photon source also has to be stable, bright, and fast. Here, stable means that the source does not blink or bleach, the brightness is the maximum rate at which single photons can be emitted (or collected), and fast means that the source has a short lived excited state.

The most important parameters quantifying the quality of a single pho-

ton source, however, are still the single photon purity and the indistinguishability. The single photon purity of the source is quantified by the dip in the intensity correlation function  $g^{(2)}(\tau)$  at zero time delay which quantifies the probability to have two photons at the same time (at  $\tau = 0$ ). The indistinguishability is quantified by a dip in the Hong-Ou-Mandel two-photon interference experiment which measures the destructive interference of two photons that arrive simultaneously at a 50:50 beam splitter.

Currently, self-assembled InAs/GaAs quantum dots perform the best overall as they are the only material system that shows single photon purities larger than 99% ( $g^{(2)}(0) < 0.01$ ) [11–14] and indistinguishability of the produced single photons of more than 90% [11, 14]. Most other material systems show increased multi photon emission with purities around 70%-90% [1].

Possibly the biggest advantage of quantum dots, however, is that they are atom-like emitters in a solid state host. This allows the quantum dot to combine the optical properties of atoms with the scalability and convenience of solid state systems [11, 15]. Moreover, quantum dots can be incorporated in optical micro cavities which increase the spontaneous emission rate due to the Purcell effect, making them a very attractive system for a fast single photon source [2].

The system we are working with is such a quantum dot coupled to an optical cavity. This is thus a system with a possible purity of  $> 99\%$  under resonant excitation and a possible indistinguishability of  $> 90\%$ . Furthermore it is stable due to the solid state environment and fast due to Purcell enhanced spontaneous emission. This conforms to the statement that these systems have the best all-round performance currently available [16–19].

There is one aspect of the ideal single photon source, however, that we did not yet mention: the brightness. We defined it earlier as “the maximal rate at which single photons can be emitted (or collected)”. The emission rate, however, is related to the lifetime of the excited state. Therefore, for a specific single emitter system, the “brightness” can only be affected by the *extraction efficiency* of single photons from the emitter. This brightness is of particular interest in this thesis: can we improve the brightness of a cavity quantum electrodynamics single photon source (a quantum dot emitter in an optical cavity) through optimizing the configuration of the input and output polarizer?

The reason for a lower collection efficiency in this system is that the most desirable form of excitation is resonantly. This is necessary to uphold the high demands on the single photon purity and indistinguishabil-

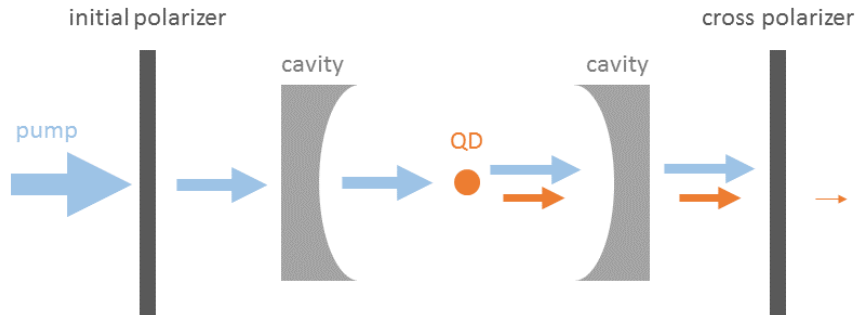


**Figure 1.1:** Schematic representation of the cavity with the quantum dot, the polarizers, and the pump (blue) and quantum dot (orange) light. Part of the light emitted by the quantum dot is filtered out by the cross polarizer, resulting in a lower transmitted than emitted single photon intensity. A brighter single photon source can be created by optimizing the polarization configuration to allow more light emitted by the quantum dot to pass through the cross polarizer while still blocking all laser light needed for the excitation of the quantum dot.

ity. With resonant excitation there are no additional relaxation processes from higher excited states necessary before the photon is emitted. This is difficult to implement practically since the single photons have to be separated from the strong excitation laser pulse [2]. One way to separate the two is by using a difference in the polarization of the light (figure 1.1). A further reason to use polarization to filter the single photons from the excitation laser pulse lies in the nature of the system used: a polarization non-degenerate quantum dot in a polarization non-degenerate cavity. A polarization non-degenerate system is a system with two modes that are split spectrally and have orthogonal linear polarization (figure 1.2), thus both the quantum dot and the cavity have two spectrally split modes with orthogonal polarization.

Since the cavity has two orthogonally polarized modes, each with a different resonance frequency, there is a natural polarization configuration to extract single photons while blocking the excitation laser pulse. This conventionally used polarization configuration consists of two crossed linear polarizers on either side of the cavity, both aligned with a different cavity mode polarization (figure 1.3). The excitation laser light is linearly polarized and aligned with one of the cavity mode polarizations by the input polarizer. This light is then blocked in transmission by the output polarizer which is aligned to the other cavity mode polarization. Since all excitation laser light is blocked, the light emitted by the quantum dot can be

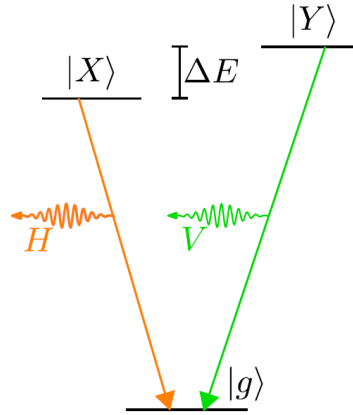


**Figure 1.2:** Schematic representation of the polarization non-degenerate modes of the quantum dot. The quantum dot has an  $X$  and an  $Y$  mode, separated in energy by  $\Delta E$  (split spectrally by the quantum dot splitting). The  $X$  mode emits horizontally polarized light and the  $Y$  mode vertically polarized light. Figure adapted from Lodahl, Mahmoodian, and Stobbe [4].

extracted because the quantum dot emits light in a different polarization (the quantum dot dipole changes the polarization of the scattered light). So how much of the emitted single photons can be extracted and collected after the output polarizer?

The output polarizer is aligned with the empty cavity mode polarization (i.e. without the excitation laser light). Therefore, the quantum dot has to emit its single photon in this empty cavity mode polarization for it to be collected. But how can the quantum dot emit in that cavity mode polarization if it is excited from the other cavity mode polarization? The polarization of the quantum dot modes is not necessarily aligned with the cavity mode polarizations. Therefore, when a quantum dot mode is excited by the excitation laser light in one cavity mode polarization, it can emit a single photon in the other cavity mode with the orthogonal polarization and this single photon can then be collected.

The polarization of the quantum dot mode has to have some overlap with both polarizations of the cavity modes in order to absorb a photon from one cavity mode and emit a photon in the other cavity mode (figure 1.3). The approach would therefore work best if the polarization of the quantum dot mode would be at  $45^\circ$  between the two cavity mode polarizations since the coupling of the two cavity mode polarizations via the quantum dot goes as  $\sin(\theta_{QD})\cos(\theta_{QD})$ . This does, however, also mean that the coupling between the cavity mode and the quantum dot mode is

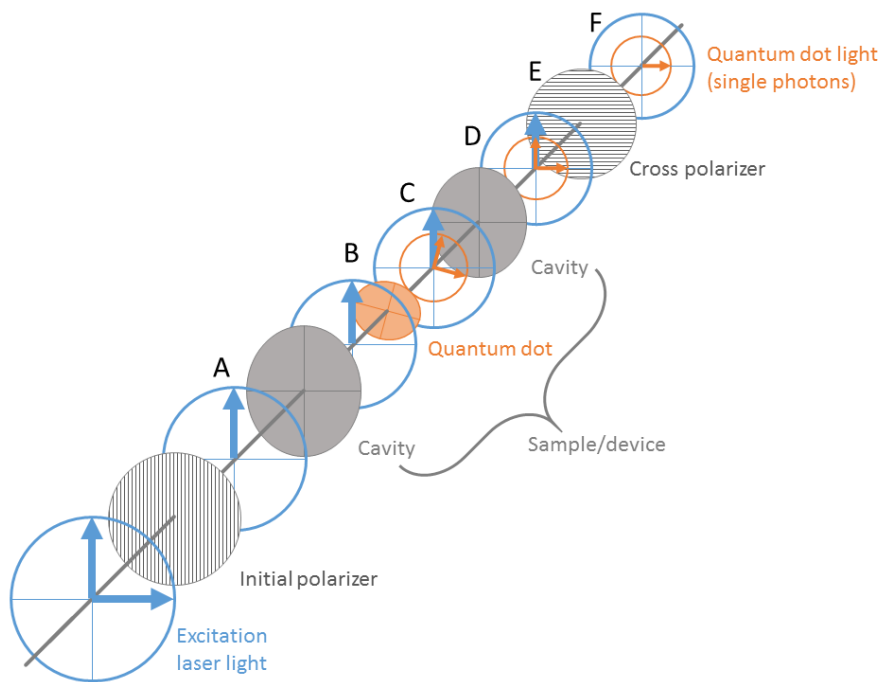


**Figure 1.3:** Schematic representation of the cavity with the quantum dot, the polarizers, and the pump (blue) and quantum dot (orange) light. Excitation laser light is vertically polarized by the input (initial) polarizer which is aligned with the polarization of one of the cavity modes (A). The polarization of the quantum dot modes is at an angle to the polarization of the cavity modes (B). The quantum dot is excited by the laser light (blue) and emits single photons (orange, C) in one of the cavity modes (D). The output (cross) polarizer blocks all excitation laser light (E) while a part of the single photons emitted by the quantum dot is transmitted (F).

only 0.5 since that goes as  $\cos(\theta_{QD})$ . For a high-brightness single photon source, a strong coupling of the polarization of the quantum dot mode to the polarization of the cavity mode is preferred and therefore a small quantum dot angle. This in turn, however, also means that the single photons emitted by the quantum dot are much more likely to be emitted in polarization of the cavity mode already filled with the excitation laser light since it goes as  $\cos^2(\theta_{QD})$  (but is possibly even higher due to stimulated emission in that cavity mode). The photons emitted in this filled cavity mode polarization, however, cannot be filtered from the excitation laser light and thus cannot be collected as single photons. Therefore, even though the coupling between the polarization of the quantum dot mode and the polarization of the cavity mode is strong, a small quantum dot angle should also result in a low brightness of the single photon source since all light in the filled cavity mode polarization is blocked by the output polarizer.

Due to our fabrication process, quantum dot mode polarizations are generally at a small angle to the cavity mode polarizations. As explained, this is clearly a non-ideal situation. It is for this reason that we want to try to optimize the polarization configuration of the input and output polarizer to block less of the single photons emitted by the quantum dot and thus produce a brighter single photon source.

## Theory and simulation

We want to fabricate a single photon source and therefore use a quantum dot in a cavity. We use an input and output polarizer in cross polarization to filter out the single photons from the excitation laser light. However, the output polarizer inherently also blocks some single photons. Therefore we want to optimize the polarization configuration in order to produce a brighter (better) single photon source.

The parameter space of the polarization configuration is so large, that it is not doable to try to optimize the polarization configuration directly in the lab. We will first study the system of a polarization non-degenerate quantum dot in a polarization non-degenerate cavity numerically in the semi classical approximation to find out if a better polarization configuration exists. We will define the optimal configuration as a configuration where, for a certain laser frequency, the intensity without the quantum dot is practically zero, while the intensity with the quantum dot is high. For this definition, there exist more optimal polarization configurations and we will try two of these configurations in the lab in chapter 4.

### 2.1 Semi-classical model

Single photons are inherently quantum since they are quantized. A full quantum description of our system, however, is beyond the scope of this thesis, but moreover, turns out not to be necessary to find the optimal polarization configuration. We will therefore use the semi classical approximation to simulate the behavior of a polarization non-degenerate quantum dot in a polarization non-degenerate cavity.

### 2.1.1 Formula

There are multiple formulas for the description of a quantum dot in a cavity, all with their own notation and choice of variables. For the simulation we will go with the formula from the thesis of Morten P. Bakker [20–23]:

$$t = \eta_{out} \frac{1}{1 - i\Delta + \frac{2C}{1 - i\Delta'}} \quad (2.1)$$

with  $t$  the transmission,  $\eta_{out}$  the output coupling efficiency,  $\Delta = 2(\omega_{laser} - \omega_{cavity})/\kappa$  the dimensionless relative detuning between the laser and the cavity (with a factor  $2/\kappa$ ),  $\Delta' = (\omega_{laser} - \omega_{QD})/\gamma_{\perp}$  the dimensionless relative detuning between the laser and the quantum dot (with a factor  $1/\gamma_{\perp}$ ), and  $2C = g^2 \times 2/\kappa \times 1/\gamma_{\perp}$  the device cooperativity with  $g$  the quantum dot mode coupling strength,  $\kappa$  the total intensity damping of the cavity and  $\gamma_{\perp}$  the quantum dot dephasing rate.

This formula depends thus on the four intrinsic sample parameters:  $\eta_{out}$ ,  $2/\kappa$ ,  $1/\gamma_{\perp}$ , and  $g^2$  and on the two resonance frequencies  $\omega_{cavity}$  and  $\omega_{QD}$  of the cavity and the quantum dot, all of which we can find from experiments.

This formula, however, does not yet take the polarization non-degeneracy of the quantum dot and the cavity into account. To incorporate the polarization we replace the scalars with 2x2 matrices. We assume equal reflection and transmission coefficients for the two cavity mode polarizations as well as equal decay rates. The line width of the quantum dot modes is assumed equal as well, so that the difference between both the cavity and the quantum dot modes is given solely by their resonance frequency. We rewrite the formula above with 2x2 matrices and with the division becoming a matrix inversion:

$$t_{2x2} = \eta_{out} \left( I_{2x2} - \begin{pmatrix} i\Delta_H & 0 \\ 0 & i\Delta_V \end{pmatrix} + R_{-\theta_{QD}} \begin{pmatrix} \frac{2C}{1 - i\Delta'_X} & 0 \\ 0 & \frac{2C}{1 - i\Delta'_Y} \end{pmatrix} R_{\theta_{QD}} \right)^{-1} \quad (2.2)$$

with  $t_{2x2}$  denoting the 2x2 transmission matrix,  $I$  the identity matrix, and  $A^{-1}$  a 2x2 matrix inversion of matrix  $A$ . Furthermore,  $\Delta_{H(V)}$  is the dimensionless relative detuning between the laser and the horizontally (vertically) polarized cavity mode (still with a factor  $2/\kappa$ ),  $\Delta'_{X(Y)}$  the dimensionless relative detuning between the laser and the X(Y)-quantum dot mode (still with a factor  $1/\gamma_{\perp}$ ) and  $R_{\theta} = \begin{pmatrix} \cos(\theta) & -\sin(\theta) \\ \sin(\theta) & \cos(\theta) \end{pmatrix}$  the rotation matrix for an angle  $\theta$ , to incorporate the rotation of the quantum dot system by an angle  $\theta_{QD}$  with respect to the polarization of the cavity modes.

This adjusted formula effectively adds only one extra factor which is the angle  $\theta_{QD}$  between the cavity frame and the quantum dot frame. Although this angle might not seem to be very interesting, we will find that it has a mayor influence on the possible quality of the single photon source and we will therefore discuss its importance in sections 2.3.1 and 2.4.2.

### 2.1.2 Limits

The semi classical model breaks down due to saturation. This saturation is governed by a dimensionless parameters given in the paper by Armen and Mabuchi [24]. The critical photon number is a measure for the amount of photons needed to saturate the response of the quantum dot:

$$n_0 = \frac{\gamma_{\parallel}\gamma_{\perp}}{4g^2} \quad (2.3)$$

with  $\gamma_{\parallel}$  the dissipative relaxation rate in modes other than the preferred cavity mode and  $\gamma_{\perp} = \gamma_{\parallel}/2 + \gamma_{nr}$  the quantum dot dephasing rate and  $g^2$  the quantum dot mode coupling strength. These rates and the coupling strength depend on the specific system and saturation of the quantum dot is reached for  $n_0 < 1$ . For the quantum dot in the cavity, the simulation holds thus for very low photon numbers in the cavity only. This means that we will need a very low power of the exciting laser light in order to not saturate the quantum dot.

## 2.2 Parameters

Some of the parameters used in the simulation have been addressed briefly in the previous section: the two frequencies of the cavity modes, the two frequencies of the quantum dot modes and the quantum dot angle. We will not refer any further to the intrinsic sample parameters ( $\eta_{out}$ ,  $2/\kappa$ ,  $1/\gamma_{\perp}$ , and  $g^2$ ) in this thesis and focus solely on the three sample dependent parameters: cavity splitting, quantum dot splitting, and quantum dot angle since these parameters can be tuned in sample fabrication. These are thus the important parameters in the system of a polarization non-degenerate quantum dot in a polarization non-degenerate cavity. We are also specifically interested in the configuration of the input and output polarizers, which is why another set of parameters is needed to describe those.

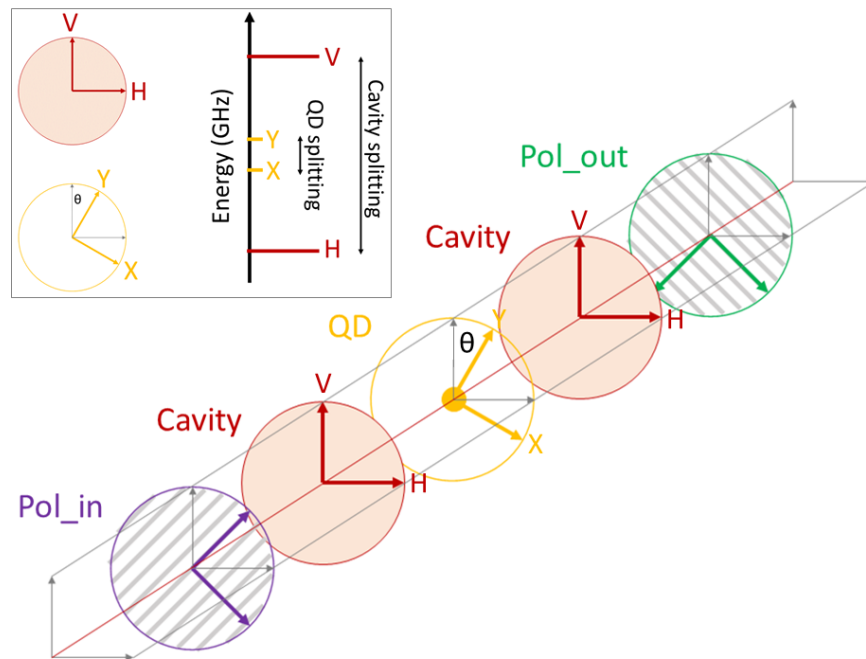


**Figure 2.1:** Schematic of the components and angles used in the semi classical simulation of a quantum dot in a cavity. The orthogonal polarizations of the cavity modes double as the axes of the reference frame. The polarization angle is defined as the angle the polarizers make with respect to the cavity axes (reference frame). The modes of the cavity (quantum dot), labeled by H (X) and V (Y), are orthogonal in polarization and spectrally separated by the cavity (QD) splitting. By convention, the energies of the cavity (quantum dot) modes is defined such that the V (Y) mode has a higher energy than the H (X) mode. The quantum dot system is rotated by an angle  $\theta_{QD}$  with respect to the cavity axes (reference frame).

A schematic of the components and angles used in the semi classical simulation of the polarization non-degenerate quantum dot in the polarization non-degenerate cavity is shown in figure 2.1. As can be seen from equation 2.2, the cavity axes are used as the reference frame for the polarization. The center between the frequency of the two cavity modes is therefore also defined to be 0 GHz and thus our reference laser frequency. Furthermore, the X mode of the cavity is defined to be lower in energy than the Y mode and similarly is the H mode of the quantum dot defined to be lower in energy than the V mode.

The list of tunable parameters used in the simulation is split in a part for the quantum dot in the cavity system and a part for the polarization. The first consists of 6 parameters and the latter of 5:

- flaser:  
the laser frequency relative to the center of the two cavity modes. The center between the two cavity modes is defined as 0 GHz and thus our reference laser frequency.
- cavsplitt:  
the frequency difference between the two cavity modes.
- QDsplit:  
the frequency difference between the two quantum dot modes.
- QDdetuning:  
the frequency of the center between the two quantum dot modes relative to the center between the two cavity modes.
- thetaQD:  
the angle between the cavity frame and the quantum dot frame.
- withQD:  
a Boolean that determines whether we compute the transmission with or without a quantum dot present in the cavity. This allows us to determine the so called quantum dot contrast: the difference in transmitted intensity with and without a quantum dot present.
- polina, polinb, polouta, poloutb:  
two scalars per polarization to store the input polarization  $\vec{e}_{in}$  and the output polarization  $\vec{e}_{out}$ . The formula used is given by:

$$\vec{e}_{in} = \frac{1}{\sqrt{1 + \text{polina}^2 + \text{polinb}^2}} \begin{pmatrix} 1 \\ \text{polina} + i \cdot \text{polinb} \end{pmatrix} \quad (2.4)$$

- `withpolarout`:  
a Boolean that determines whether we compute the transmission with or without an output polarizer present. This allows us to simulate the total transmission which is useful to compare to polarization scan experiments.

Some of these parameters are adjustable in the lab while others are sample dependent. We can change `flaser` with the scanning laser, `QDdetuning` and `withQD` through the bias voltage on the PIN junction, and of course the 5 polarization parameters. The three sample dependent parameters, `cavsplit`, `QDsplit`, and `thetaQD`, can be found through analysis of a polarization scan of the sample.

## 2.3 Understanding the model

Now that we have found a way to simulate the behavior of the quantum dot in the cavity as a function of the input and output polarizers, we will elaborate some more on two of the sample dependent parameters: the quantum dot angle and the cavity splitting. First we will look at the quantum dot angle and see that it has a profound effect on the brightness of the single photon source and that the angle has a  $180^\circ$  rather than a  $90^\circ$  rotational symmetry. Secondly we will see that the cavity splitting plays a major role in the polarization of the transmitted light through the cavity due to birefringence induced by the spectrally split cavity modes.

### 2.3.1 Quantum dot angle near $0^\circ$ or $90^\circ$

At first sight, a quantum dot angle of  $\theta_{QD} = 0^\circ$  or  $\theta_{QD} = 90^\circ$  should not make a difference since the cavity mode polarizations and quantum dot mode polarizations overlap in either case. There is a subtle difference, however, which comes from the non-degeneracy of the cavity and quantum dot mode polarizations. Around  $\theta_{QD} = 0^\circ$ , the X mode of the quantum dot interacts with the H mode of the cavity (by definition of the quantum dot angle, see figure 2.1) while for  $\theta_{QD} = 90^\circ$ , the X mode of the quantum dot interacts with the V mode of the cavity. These modes, X and Y for the quantum dot and H and V for the cavity, are split spectrally (and thus in energy). We have defined the X mode to be lower in energy than the Y mode and similarly the H mode to be lower in energy than the V mode. Therefore, around a quantum dot angle of  $\theta_{QD} = 0^\circ$  the low energy quantum dot mode interacts mainly with the low energy cavity mode and the

high energy quantum dot mode with the high energy cavity mode. In contrast, around  $\theta_{QD} = 90^\circ$  the low energy quantum dot mode interacts mainly with the high energy cavity mode and vice versa for the high energy quantum dot mode. Although this might seem like a trivial difference, it turns out to greatly affect the maximal brightness of a single photon source in such a system.

The total transmission due to the polarization non-degenerate quantum dot is enhanced for a quantum dot splitting up to about 4 GHz when the quantum dot angle is near  $\theta_{QD} = 0^\circ$  and reduced when the angle is near  $\theta_{QD} = 90^\circ$ . This is due to the effect the quantum dot has on the phase of the light in the cavity. The quantum dot effectively adds a phase to the light with which it interacts, thus causing light of a different frequency to fit more optimally in the cavity mode. This is illustrated in figure 2.2. The cavity mode is shown in grey dashes and the cavity mode with a quantum dot in the cavity is shown in red. A dip is visible at the frequency of the quantum dot mode since the light is absorbed by the quantum dot mode at that frequency. A Fano like peak is visible at a slightly higher frequency (for the lower energy cavity mode): the light picks up a phase from the quantum dot which causes the light at that frequency to fit more optimally in the cavity than without the quantum dot present.

If we think of the effect the quantum dot mode has on the cavity mode as if it pushes part of the light in the cavity mode spectrally outward, we can understand the difference between a quantum dot angle of  $\theta_{QD} = 0^\circ$  and  $\theta_{QD} = 90^\circ$  more easily. Recall that the X and the H mode are defined to be lower in frequency (energy) than the Y and V modes. Around  $\theta_{QD} = 0^\circ$ , the Fano like peaks are pushed towards each other resulting in a peak (figure 2.2 left). Around  $\theta_{QD} = 90^\circ$ , however, the Fano like peaks are pushed away from each other resulting in a relative dip (figure 2.2 right).

Based on the above results, we would like our sample to have a quantum dot angle around  $\theta_{QD} = 0^\circ$  for a bright single photon source. We will see that this is partly true as the optimal quantum dot angle lies between  $\theta_{QD} = 5^\circ$  and  $\theta_{QD} = 50^\circ$  for low quantum dot splitting which is definitely closer to  $\theta_{QD} = 0^\circ$  than to  $\theta_{QD} = 90^\circ$ .

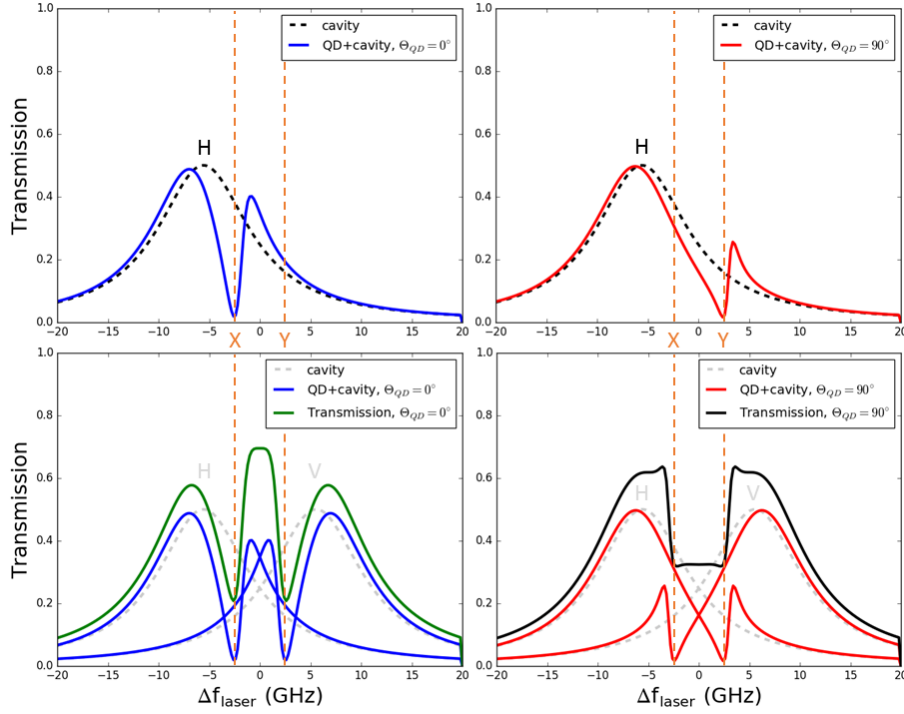


**Figure 2.2:** Simulation of the system with the quantum dot angle at  $\theta_{QD} = 0^\circ$  (left) and at  $\theta_{QD} = 90^\circ$  (right). The input polarizer is set to  $\theta_{pol} = 45^\circ$  (both cavity modes are excited equally) for all plots. The output polarizer is set to different settings for the different plots. (top): the output polarizer is set to  $\theta_{pol} = 0^\circ$ . (bottom, blue and red curves): the output polarizer is set to  $\theta_{pol} = 0^\circ$  and  $\theta_{pol} = 90^\circ$ . (bottom, green and black curves): no output polarizer is used. For  $\theta_{QD} = 0^\circ$  (left), the H (V) mode of the cavity interacts with the X (Y) mode of the quantum dot (top) and the Fano like line shapes created by the quantum dot overlap resulting in a peak in total transmission (bottom). For  $\theta_{QD} = 90^\circ$  (right), the H (V) mode of the cavity interacts with the Y (X) mode of the quantum dot (top), shifting the Fano like line shapes resulting in a relative dip in total transmission (bottom).

### 2.3.2 Cavity mode splitting

The goal of the output polarizer is to stop the coherent excitation laser light from being transmitted (or all light when no quantum dot mode is present in the cavity). Therefore, to find a possibly more optimal configuration, we decided to look into the polarization of the light coming out of the cavity. This polarization depends mainly on two parameters: the polarization of the incoming light and the cavity splitting (how much the cavity modes are split spectrally).

Firstly we looked at horizontal and vertical input polarization. For horizontal input polarization, only horizontal polarized light will exit the cavity because it will only interact with the horizontally polarized cavity mode. The polarization does thus not depend on the cavity splitting and the same story holds for vertically polarized light. This is why a polarization configuration with a horizontal linear input polarizer and a vertical linear output polarizer blocks the excitation laser light. We will refer to this polarization configuration as **90Cross** since the linear input and output polarizers are cross polarized at an angle of  $90^\circ$  to each other.

The second logical input polarization is for an input polarization exactly between the polarizations of the cavity modes: a linear polarizer at  $45^\circ$  to the H or V mode of the cavity. For this input polarization, the polarization of the light coming out of the cavity does depend on the cavity splitting (figure 2.3).

At a cavity splitting of 0 GHz, the cavity is polarization degenerate and thus does not change the polarization of the incoming light. At higher cavity splitting, however, the cavity becomes birefringent due to the frequency mismatch between the horizontally and vertically polarized cavity modes. This birefringence causes the diagonally polarized light to pick up a circular component. The light exiting the cavity is nearly circular around a cavity splitting of 11 GHz for the parameters of our samples and scales with the total intensity damping factor of the cavity  $\kappa$ . The samples in the lab have a cavity splitting of around 10 GHz and the outgoing polarization is thus still pretty close to circular for an incoming polarization of  $45^\circ$ . When simulated, this polarization configuration showed a higher intensity with the quantum dot present than the 90Cross polarization configuration. This  $45^\circ$  in, circular out polarization configuration apparently blocks less of the single photons emitted by the quantum dot while it is still a configuration that should be relatively easy to reproduce in the lab. We will refer to this polarization configuration as **45Circ**.

There is thus a polarization configuration (45Circ) that yields a possibly brighter single photon source than the conventionally used polarization

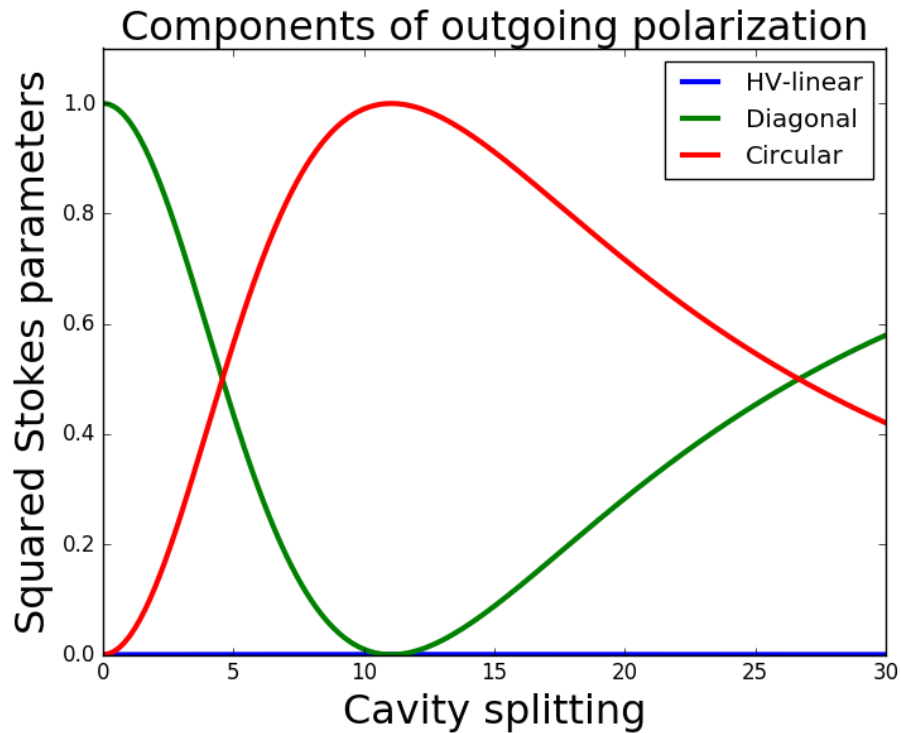


**Figure 2.3:** Polarization components as given by the Stokes parameters of the light exiting the cavity for an input polarization of  $45^\circ$  to the H or V mode of the cavity at a laser frequency centered exactly between the two cavity modes as a function of splitting of the cavity modes. The light has no horizontal or vertical component for any cavity splitting (HV-linear). The light is diagonally polarized for 0 GHz cavity splitting since the cavity is then polarization degenerate and thus does not change the polarization. With a non-zero cavity splitting, the cavity is birefringent and thus changes the relative phase between the horizontally and vertically polarized light. Around 10 GHz cavity splitting, the light is circularly polarized due to this birefringence of the cavity.

configuration (90Cross). This also means that there is probably an even better polarization configuration possible. That configuration, however, will most likely have a polarization of elliptical nature which makes it difficult to find solely through manual analysis of the simulation results. In order to find such a configuration, we will therefore run an optimization algorithm over the set of parameters that we can tune in the lab.

## 2.4 Optimal polarization configuration

The standard polarization configuration with two crossed linear polarizers (90Cross) apparently blocks some of the single photons generated by the quantum dot. There is another polarization configuration (45Circ) that also blocks the excitation laser light, but allows more light emitted by the quantum dot to pass through the output polarizer. This strengthens our belief that an even more optimal polarization configuration can be found. We will thus run an optimization algorithm over the lab adjustable parameters (polarization configuration, detuning of the quantum dot, and laser frequency), for the range of parameters set by the sample (cavity splitting, quantum dot splitting, and quantum dot angle). As stated previously, the optimal configuration is a configuration where, for a certain laser frequency, the intensity without the quantum dot is practically zero, while the intensity with the quantum dot is high. Based on this definition, we used an adjusted visibility as the valuation function:

$$\text{valuation} = \frac{I_{\text{withQD}} - (I_{\text{noQD}} + \text{offset})}{I_{\text{withQD}} + (I_{\text{noQD}} + \text{offset})} \quad (2.5)$$

with  $I_{\text{withQD}}$  the transmitted intensity with a quantum dot present,  $I_{\text{noQD}}$  the transmitted intensity without a quantum dot present, and  $\text{offset}$  an offset to the intensity without a quantum dot. The offset is added because the visibility is maximal when the intensity without a quantum dot is zero, while that does not necessarily result in a bright single photon source.

To find the global minimum in the 6-dimensional parameter space of the polarization configuration (4), quantum dot detuning, and laser frequency, we used a combination of two algorithms: Nelder-Mead to find a (local) minimum and Basin Hopping to jump out of a local minimum in order to find the global minimum. We found that this resulted in the optimization algorithm finding the global minimum nearly every time for each of the parameters set by the sample. Since the parameters were unbounded, the algorithm occasionally ran off to some local minimum (for quantum dot angles near  $0^\circ$ ,  $45^\circ$  or  $90^\circ$ ). The global minimum, however,

shows a definite trend as a function of the parameters set by the sample and therefore we can easily discern between points where a local minimum was found and points where the global minimum was found. We will therefore ignore the erroneous pixels where a local minimum was found in the plots shown below (figures 2.4 - 2.7).

As stated above, the optimization algorithm searches the set of lab adjustable parameters for a configuration where the intensity with the quantum dot is highest while the intensity without the quantum dot is practically zero. The algorithm then returns the values for the intensity with and without a quantum dot, but it also gives the set of lab adjustable parameters for those intensities.

Although the total transmitted intensity as a function of the parameters set by the sample is interesting, we cannot change these parameters in the lab. We will therefore first look into the input and output polarization as a function of these parameters, since this thesis focuses on optimizing the polarization configuration. We will see that the input and output polarization is identical apart from a complex conjugation. Furthermore, the polarization configuration does not depend on the quantum dot splitting or on the quantum dot angle and that only the phase between the horizontal and vertical polarization depends on the cavity splitting.

After we have analyzed the optimal polarization configuration, we will look at the optimal sample dependent parameters (cavity splitting, quantum dot splitting, and quantum dot angle). We will see that an optimal sample would have a cavity splitting of 5-15 GHz, a quantum dot splitting larger than 1 GHz and a quantum dot angle of  $\theta_{QD} = 20^\circ - 60^\circ$ .

The above only holds, however, if the polarization configuration found by the optimization algorithm does indeed produce better results than the conventional polarization configuration for the sample in the lab. This sample lies somewhere in the three dimensional space of sample dependent parameters (cavity splitting, quantum dot splitting, and quantum dot angle), and if the optimal polarization configuration yields a brighter single photon source there, it should do so over the whole range of sample dependent parameters since the polarization configuration is nearly identical through this three dimensional space.

### 2.4.1 Polarization (lab adjustable parameter)

In the simulation, the input (output) polarization is parameterized in two scalars called polina (polouta) and polinb (poloutb). These scalars are not very intuitive but necessary since the optimization algorithm would oth-

erwise find non-physical optimal solutions in the rounding off error of the sin or cosine. In order to return to a more intuitive set of parameters, the polarization was reparameterized into two different scalars  $\theta$  and  $\phi$  via:

$$\vec{e}_{in} = \begin{pmatrix} \sin\theta \\ \cos\theta e^{i\phi} \end{pmatrix} \quad (2.6)$$

where  $\theta$  determines factor of horizontally and vertically polarized light and  $\phi$  the phase between them. To get a feeling of how this parameterization of the polarization works, we will give some examples. For horizontally or vertically polarized light ( $\theta = 0^\circ$  or  $90^\circ$ )  $\phi$  is undefined, because it describes an irrelevant global phase. For diagonally polarized light  $\theta = 45^\circ$  and  $\phi = 0^\circ$ , and finally, for circularly polarized light  $\theta = 45^\circ$  and  $\phi = 90^\circ$ .

As we can see from figure 2.4, the optimal polarization configuration is almost completely independent of two of the three parameters set by the sample: the quantum dot splitting and the quantum dot angle. Furthermore, the input and output polarization seem to be identical. The simulation, however, does still take the complex conjugate of the output polarization, so the input and output polarization are actually each other's complex conjugate. This shows up, however, only in the phase between the horizontally and vertically polarized light: the phase is identical but opposite in sign for the input and the output polarization.

As we can see from figure 2.5, the optimal polarization configuration does depend on the cavity splitting of the sample, but it does so only in the phase factor  $\phi$  and not in the factor of horizontally and vertically polarized light  $\theta$ . This factor of horizontally and vertically polarized light is more or less equal ( $\theta \approx 45^\circ$ ) for all parameters set by the sample. Since this factor of horizontally and vertically polarized light is more or less equal, the phase between these polarizations essentially determines the circularity of the light. As we have seen, a phase of  $0^\circ$  corresponds with diagonal light and a phase of  $90^\circ$  with circular light. Therefore, the optimal polarization configuration is elliptical in and counter elliptical out with the circularity decreasing with increasing cavity splitting.

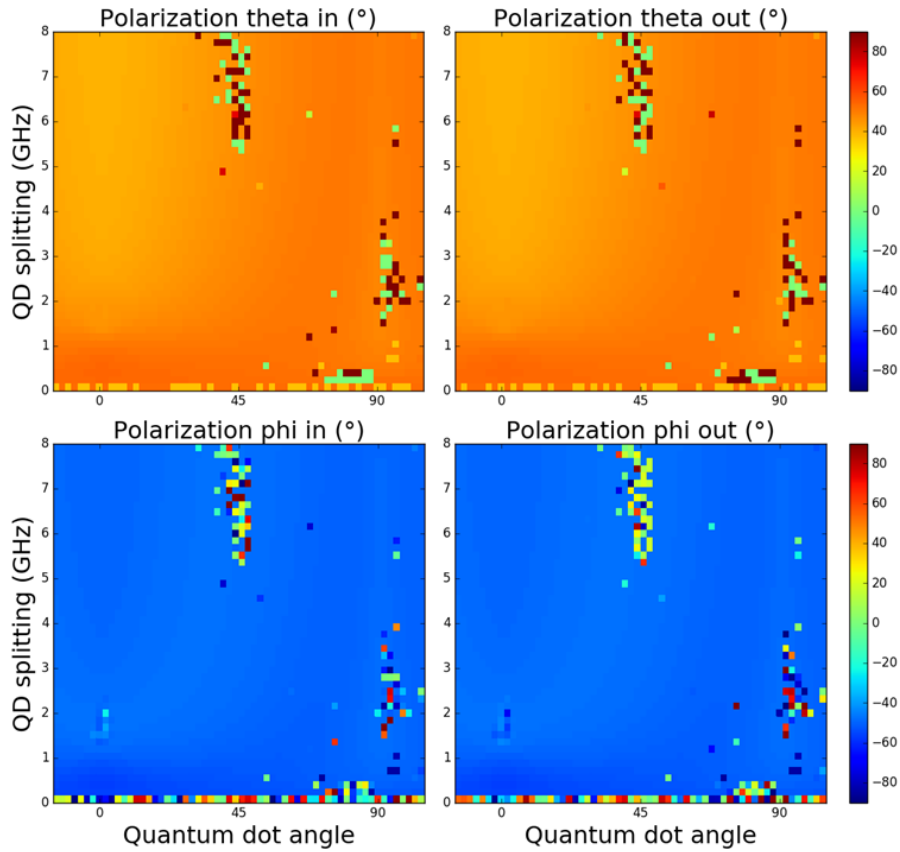


**Figure 2.4:** 2D plots of the polarization angles  $\theta$  and  $\phi$  of the input and output polarization as found by the optimization algorithm as a function of quantum dot angle and quantum dot splitting at a cavity splitting of 10 GHz.  $\theta$  determines the factor of horizontally and vertically polarized light and  $\phi$  determines the phase between these two polarizations. The color scale goes from  $-90^\circ$  to  $+90^\circ$  with  $\theta$  close to  $45^\circ$  ( $\pm 7^\circ$ ) everywhere, corresponding to an equal amount of vertically and horizontally polarized light.

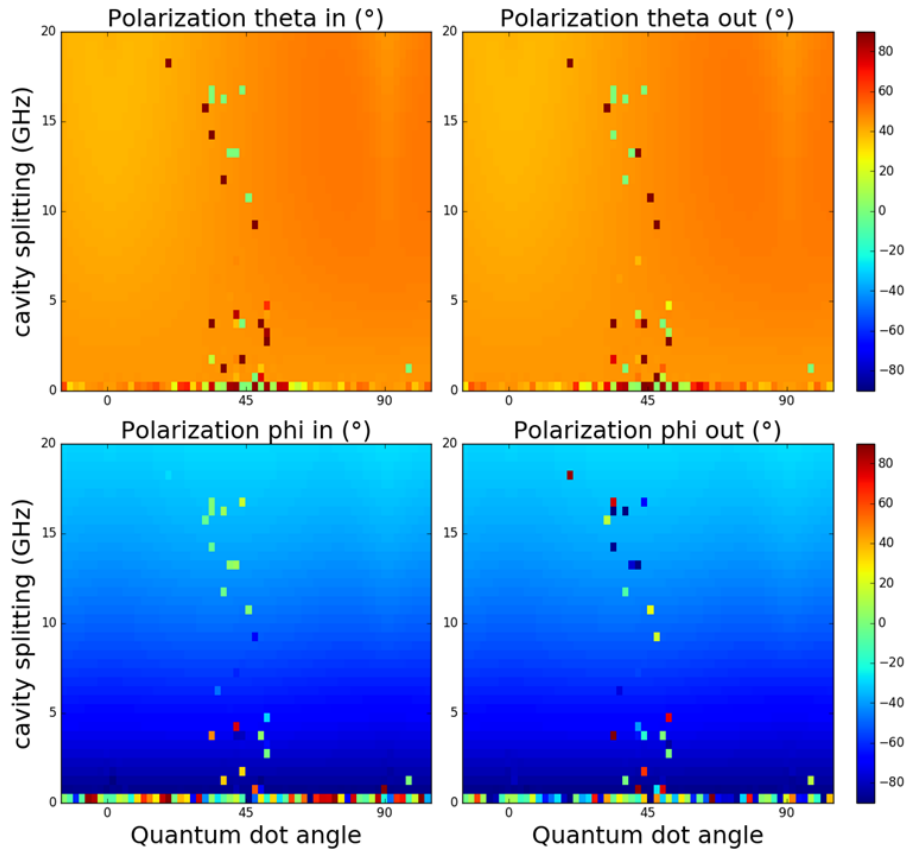


**Figure 2.5:** 2D plots of the polarization angles  $\theta$  and  $\phi$  of the input and output polarization as found by the optimization algorithm as a function of quantum dot angle and cavity splitting at a quantum dot splitting of 5 GHz. The color schale goes from  $-90^\circ$  to  $+90^\circ$  with  $\theta$  close to  $45^\circ$  ( $\pm 7^\circ$ ) everywhere, corresponding to an equal amount of vertically and horizontally polarized light. The phase  $\phi$  between the two polarizations depends on the cavity splitting and effectively determines the circularity of the polarization since the  $\theta$  is close to  $45^\circ$  everywhere.

### 2.4.2 Sample dependent parameters

As stated above, the simulation returns the maximal intensity with the quantum dot for a certain polarization configuration with practically zero intensity (order  $1\text{E-}5$  for the optimal configuration) without a quantum dot in the cavity. We can look at this intensity with the quantum dot as the maximal possible brightness of the single photon source. This intensity is plotted as a function of the three sample dependent parameters in figures 2.6 and 2.7: cavity splitting, quantum dot splitting, and quantum dot angle.

We find from these figures that the maximal intensity is limited to about 0.4 on a scale of 0 to  $\eta_{out}$  (the output coupling efficiency). (The intensity of a single cavity mode is 1 on this scale when the input polarization is aligned with this mode and no output polarizer is used (or if the output polarizer is aligned to that cavity mode polarization as well).) This is thus an upper limit to the brightness of the single photon source if we want to resonantly excite the quantum dot and thus use a polarizer to filter the excitation laser light.

Furthermore, the transmitted intensity is high for a cavity splitting of about 5-15 GHz. The quantum dot splitting and the quantum dot angle are a little mutually dependent for a quantum dot splitting up to 4 GHz. The transmitted intensity is high for a quantum dot angle of about  $20^\circ$ - $60^\circ$  for a quantum dot splitting higher than 6 GHz, but decreases with decreasing quantum dot splitting down to 1 GHz where the maximal intensity drops significantly. An optimal sample would thus have a cavity splitting of 5-15 GHz, a quantum dot splitting larger than 1 GHz and a quantum dot angle of  $20^\circ$ - $60^\circ$ .

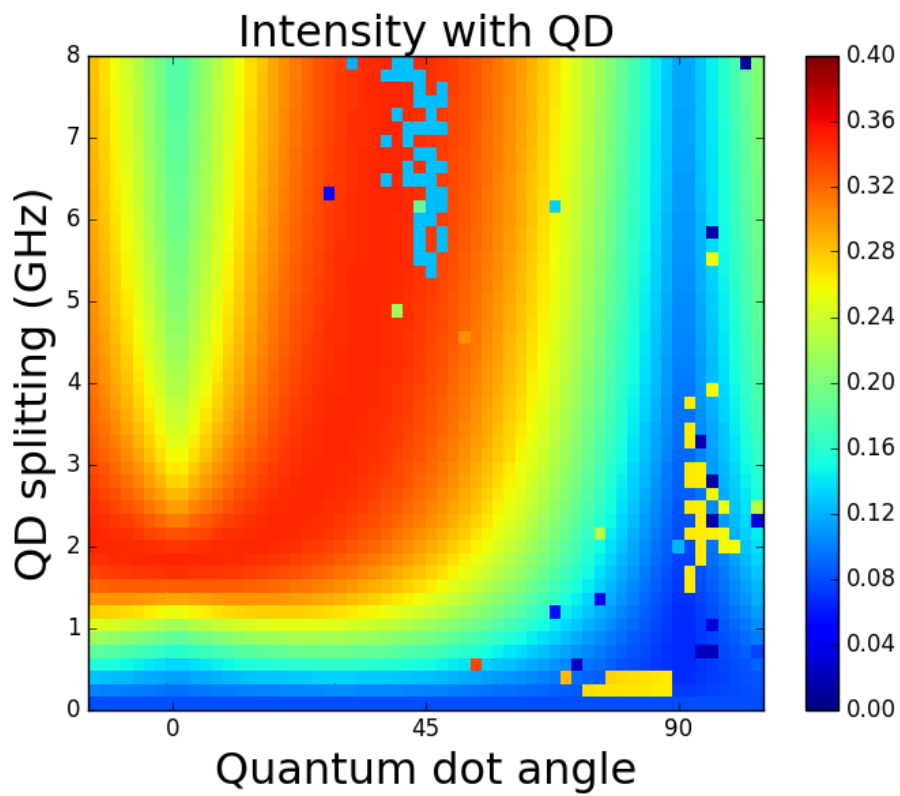


**Figure 2.6:** A 2D plot of the transmitted intensity with a quantum dot in the cavity as a function of quantum dot angle and quantum dot splitting at a cavity splitting of 10 GHz for the optimal settings as found by the optimization algorithm.

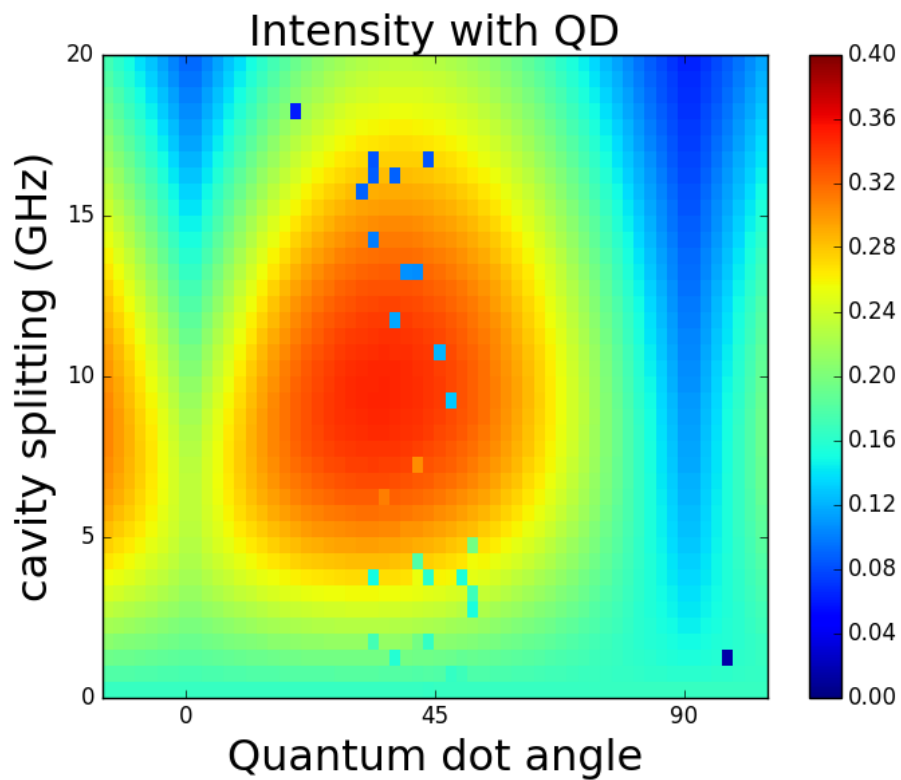


**Figure 2.7:** A 2D plot of the transmitted intensity with a quantum dot in the cavity as a function of quantum dot angle and cavity splitting at a quantum dot splitting of 5 GHz for the optimal settings as found by the optimization algorithm.

# Materials and Methods

## 3.1 Materials

Both the setup and the sample are very intricate and complicated, but we will describe both without much detail in this chapter and focus on the aspects important for this thesis only. For more info on the setup and the sample we refer to the thesis of M.P. Bakker [20] or the more recent paper by Snijders et al. [25].

### 3.1.1 Experimental setup

A schematic of the experimental setup is shown in figure 3.1. The scanning laser is a tunable near infrared laser with a wavelength regime of 930-945 nm, and a spectral width smaller than 1 MHz. The input and output polarizer are linear polarizers with an extinction ratio of  $10^4$ , accompanied by quarter wave plates to produce the circular and elliptical polarizations necessary in this thesis. The sample is located in a cold finger cryostat that keeps the sample at 5 K. The 20x objectives are used to focus the light in this cryostat. Transmitted light is detected by single photon detectors with a detection efficiency around 930 nm of 22%, a detection jitter of 500 ps, and a dark count rate of 100 cps.

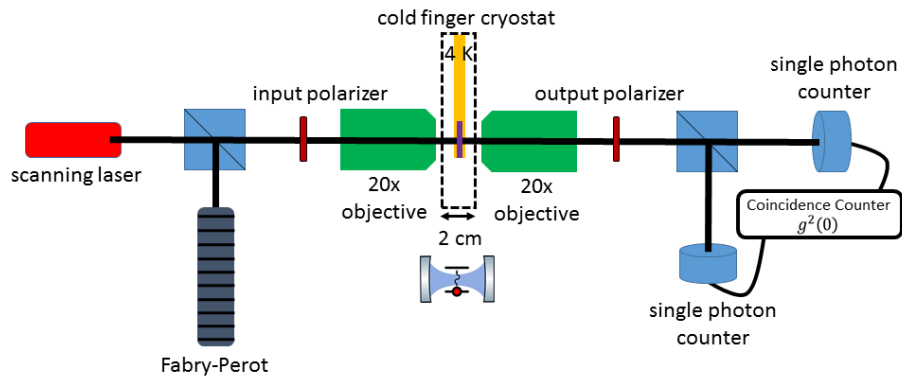


**Figure 3.1:** Schematic of the measurement setup. The sample with the quantum dot is located in the cold finger cryostat. The frequency of the scanning laser is locked to a Fabry-Perot. The output polarizer is in cross polarization with the input polarizer to filter out the incoming laser light. The single photon counters are connected to a coincidence counter that generates the intensity correlation function  $g^{(2)}(\tau)$ .

### 3.1.2 Sample

A schematic and a SEM image of the sample are shown in figure 3.2. The schematic shows the structure of the sample: two multi layer thin film mirrors (distributed Bragg reflectors) above and below the cavity containing InAs/GaAs self-assembled quantum dots. The oxide aperture acts as an intra-cavity lens for transverse confinement of the cavity modes. A PIN junction is used to shift the quantum dot energy by the quantum confined Stark effect (used for tuning the frequency of the quantum dot modes to the cavity modes). The SEM image shows trenches etched in the sample, necessary to produce the oxide aperture through wet chemical oxidation.

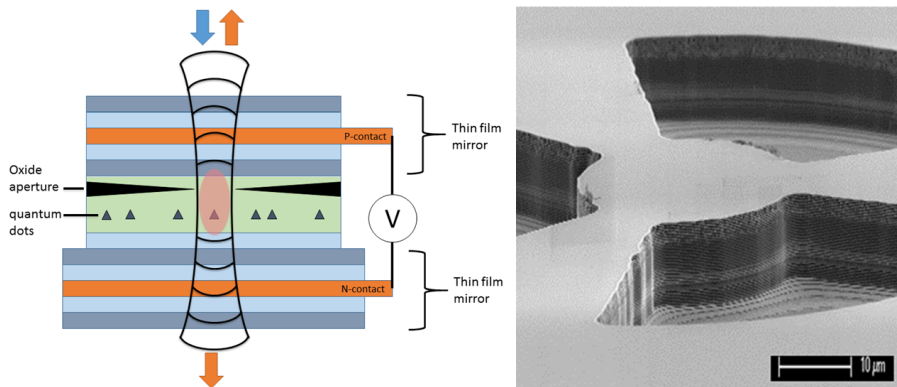


**Figure 3.2:** Schematic (left) and SEM image (right) of the sample with the cavity and quantum dots. The cavity consists of two multi layer thin film mirrors below and on top of the quantum dots. An oxide aperture is used for transverse confinement of the cavity mode. A PIN junction is used to tune the excitation frequency of the band structure of the quantum dot around the resonance frequency of the cavity. Trenches are etched in the sample to confine the light in the z-direction of the cavity.

## 3.2 Methods

The setup allows for a large set of measurements, but we will describe only the methods of the four measurements used in this thesis. Three of these depend on the ability of the laser to scan over a range of frequencies while the last needs a stable laser frequency.

### 3.2.1 Laser scan

The frequency of the scanning laser is swept over the scan range (about 80 GHz) while one of the APDs records the photons collected at each frequency. The result is a plot of the transmission intensity (in counts per second, cps) as a function of the relative laser frequency (in GHz).

### 3.2.2 Polarization scan

The input and/or output polarizer is rotated over a range of angles and a laser scan is performed for each angle. The result is a 2D plot of the transmission intensity (cps) as a function of the relative laser frequency (GHz) and the polarization angle ( $^{\circ}$ ). The input polarization angle of a linear polarizer determines the amount in which the separate cavity modes are

excited and a polarization scan allows us thus (among others) to find the axes of the cavity frame.

### 3.2.3 Voltage scan

The bias voltage over the PIN junction is swept over the scan range (about 0.2 V) and a laser scan is performed for each voltage in the scan range. This is used to shift the quantum dot energy by the quantum confined Stark effect. The result is a 2D plot of the transmission intensity (cps) as a function of relative laser frequency (GHz) and applied bias voltage (V). The bias voltage changes the excitation frequency of the quantum dot and a voltage scan allows us thus to find the voltage needed to tune the quantum dot frequency to the cavity frequency.

### 3.2.4 $g^{(2)}(\tau)$ -measurement

For photon correlation measurements, the frequency of the scanning laser is stabilized by locking it to a stable Fabry-Perot cavity. One of the APDs starts a time measurement as soon as a photon is detected while the other APD stops this measurement. This is a Hanbury-Brown and Twiss setup. The histogram of time delays between a photon detected at the start APD and the stop APD gives the temporal distribution of consecutive photon detection events. The probability to detect not the next, but any photon after a certain time is then given by the probability that this photon is the next one, plus the probability that this photon is the second one, plus etc. This probability distribution is related to the intensity correlation function  $g^{(2)}(\tau)$  by  $P(\tau) = \langle I(\tau) \rangle g^{(2)}(\tau)$ . A single photon source is characterized by photon anti-bunching which shows up in the intensity correlation function as  $g^{(2)}(0) < 1$  and a  $g^{(2)}(\tau)$  measurement allows us therefore to determine the performance of such a source.

## Experimental results and discussion

The goal of this thesis is to see whether we can improve the brightness of a cavity quantum electrodynamics single photon source through the optimization of the polarization configuration of the input and output polarizer. The simulation showed that there is a better polarization configuration possible than the conventionally used crossed linear polarizers (90Cross). This conventional polarization configuration is very easy to find in the lab while the optimal configuration as proposed by the optimization could be rather difficult to find since it is elliptical. The output polarization can be found experimentally by minimizing the transmission without a quantum dot. The elliptical input polarization is more difficult. As an alternative, we will therefore also look at the configuration that we found through analysis of the simulation results: 45° linear input polarization and circular/elliptical out (45Circ). The input polarization is easy to find because it is linear and exactly between the H and V polarized modes of the cavity. The configuration of the output polarizer can then be found experimentally by minimizing the transmitted intensity without a quantum dot.

As an aid to find the three polarization configurations in the lab, we simulate the line shapes of the laser scan for the three desired polarization configurations (for the sample dependent parameters of the sample). This line shape can then be reproduced in the lab in combination with the knowledge of the nature of the polarization that we are looking for. For such an approach, we will first need to find the cavity splitting, the quantum dot splitting and the quantum dot angle of the sample under study. Then we can simulate the line shapes for the three different desired polar-

izations and reproduce those in the lab. Finally, in order to characterize the quality of the single photon source, we will measure the photon characteristics through a  $g^{(2)}(\tau)$  measurement.

## 4.1 Sample dependent parameters

We can find the sample dependent parameters from a polarization scan (figure 4.1). The linear input polarizer is rotated over  $180^\circ$  with no output polarizer while a laser scan is performed at each frequency. This results in a 2D plot of the transmitted intensity as a function of relative laser frequency and input polarization angle. The two cavity modes will show up as large peaks and the quantum dot modes as small dips in those peaks. The cavity and quantum dot splitting can be found from the difference in relative laser frequency between the modes (that are separated  $90^\circ$  in input polarization angle). The quantum dot angle can be retrieved from the difference in angle of the maximum of the cavity mode peak and the minimum of the quantum dot dip.

From the polarization scan we extract a cavity splitting of about 10 GHz with a quantum dot splitting of about 2 GHz. To find the quantum dot angle, we fitted the peak of the cavity mode and dip of the quantum dot mode as a function of polarization angle with a Gaussian. The difference between the peak of the cavity mode and the dip of the quantum dot mode was found to be about  $4^\circ$ . As described in section 2.3.1 there is a definite difference between  $\theta_{QD} = 0^\circ$  and  $\theta_{QD} = 90^\circ$ . Therefore, to find the actual quantum dot angle, we simulated a polarization scan with a quantum dot angle of  $4^\circ$  and a quantum dot angle of  $94^\circ$ . From comparison of these simulations (figure 4.2) with the measurement data (figure 4.1), it is clear that the quantum dot angle of our sample is  $94^\circ$ . Now that we know all three sample parameters, we can simulate the line shapes of the laser scan for the three polarization configurations and then try to reproduce those in the lab.

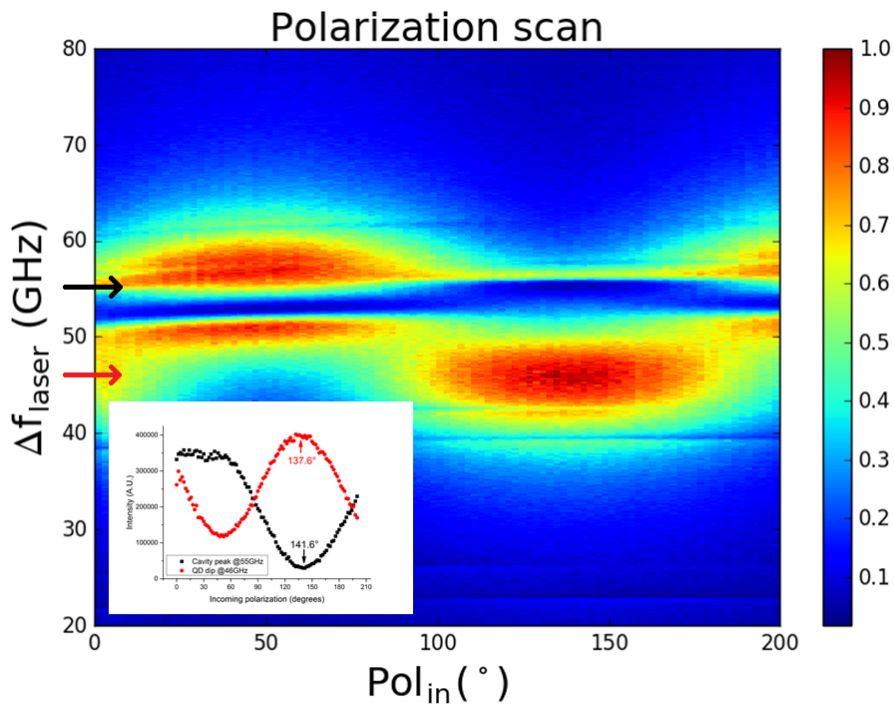


**Figure 4.1:** A measurement of the transmitted intensity without an output polarizer as a function of incoming polarization angle and laser frequency (arbitrary offset) with a quantum dot in the cavity. The inset shows the transmitted intensity as a function of incoming polarization angle for a laser frequency set to one of the cavity mode (red) and one of the quantum dot mode frequencies (black). The fit of these curves shows a relative angle difference between the two peaks of  $4^\circ$ .

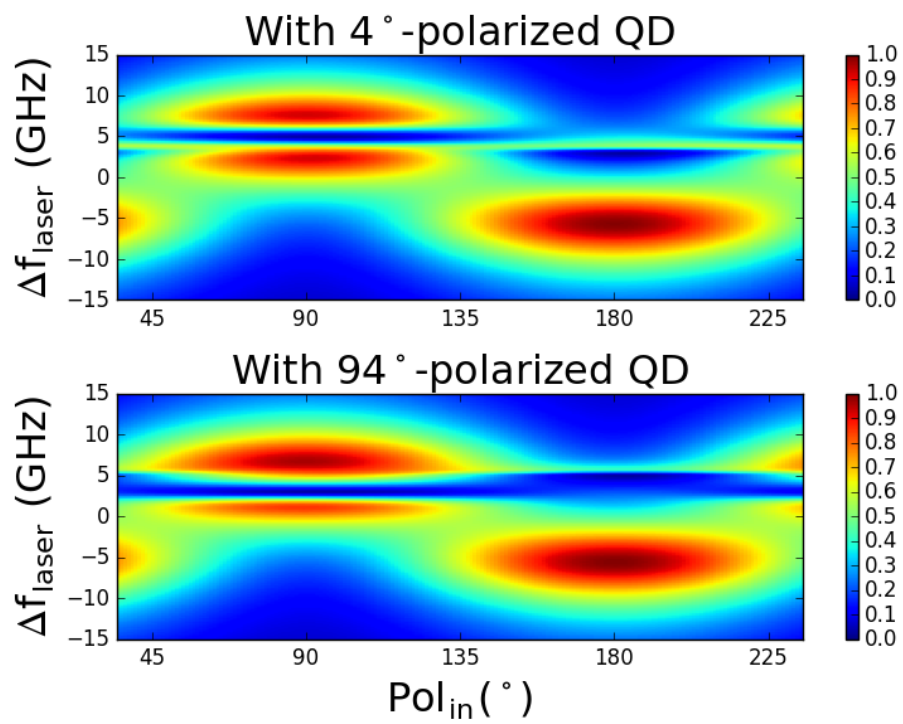


**Figure 4.2:** A simulation of the transmitted intensity without an output polarizer as a function of incoming polarization angle and relative laser frequency with a quantum dot in the cavity for a quantum dot angle of  $4^{\circ}$  and  $94^{\circ}$ .

## 4.2 Laser scan line shapes

As a tool to find the desired polarization configurations in the lab, we can simulate the shape of the laser scan for each configuration. This is most helpful for the optimal polarization configuration, but it will help to find the other two polarization configurations (45Circ and 90Cross) as well.

To recap, there are three polarization configurations that we would like to test in the lab for their brightness and quality of the single photon source. The first polarization configuration is the commonly used configuration with two crossed linear polarizers aligned with the cavity mode polarizations that we will refer to as **90Cross**. The second configuration is a linear polarizer under  $45^\circ$  to the cavity mode polarizations with an output polarizer which is nearly circular which we will refer to as **45Circ**. The third configuration is the configuration found by the optimization algorithm and consists of an elliptical in and reverse elliptical out which we will refer to as **Optimal**.

To reproduce the polarization configurations, we simulated four line shapes per configuration: two with and two without an output polarizer and both with and without a quantum dot present in the cavity. The line shapes without the output polarizer serve as a guideline for the input polarization and the two with the output polarizer serve to confirm that we have found the desired polarization configuration.

The four line shapes of the three polarization configurations were reproducible in the lab with the simple restraints that for the 90Cross configuration only linear polarizers were used, for the 45Circ one linear and one circular/elliptical polarizer was used and for the optimal configuration two elliptical polarizers were used. In practice, this means that no quarter wave plates were used for the 90Cross configuration, one quarter wave plate was placed after the sample for the 45Circ and two quarter wave plates were used to fabricate the Optimal polarization configuration.

Although the line shapes of all three polarization configurations match qualitatively, there is a quantitative difference between the simulation and the experiment for the 90Cross configuration. The simulation predicts a relative intensity between the three polarization configurations of about 1:20:30 whereas the measurement clearly shows this factor of 90Cross: 45Circ: Optimal to be about 1:2:3. We are thus either missing a factor of 10 in the simulation of the 90Cross configuration or the sample under study gives us a factor of 10 extra in intensity for this configuration. It turns out that it is the latter of the two and we will discuss the mechanism that adds the extra intensity at the end of this chapter.

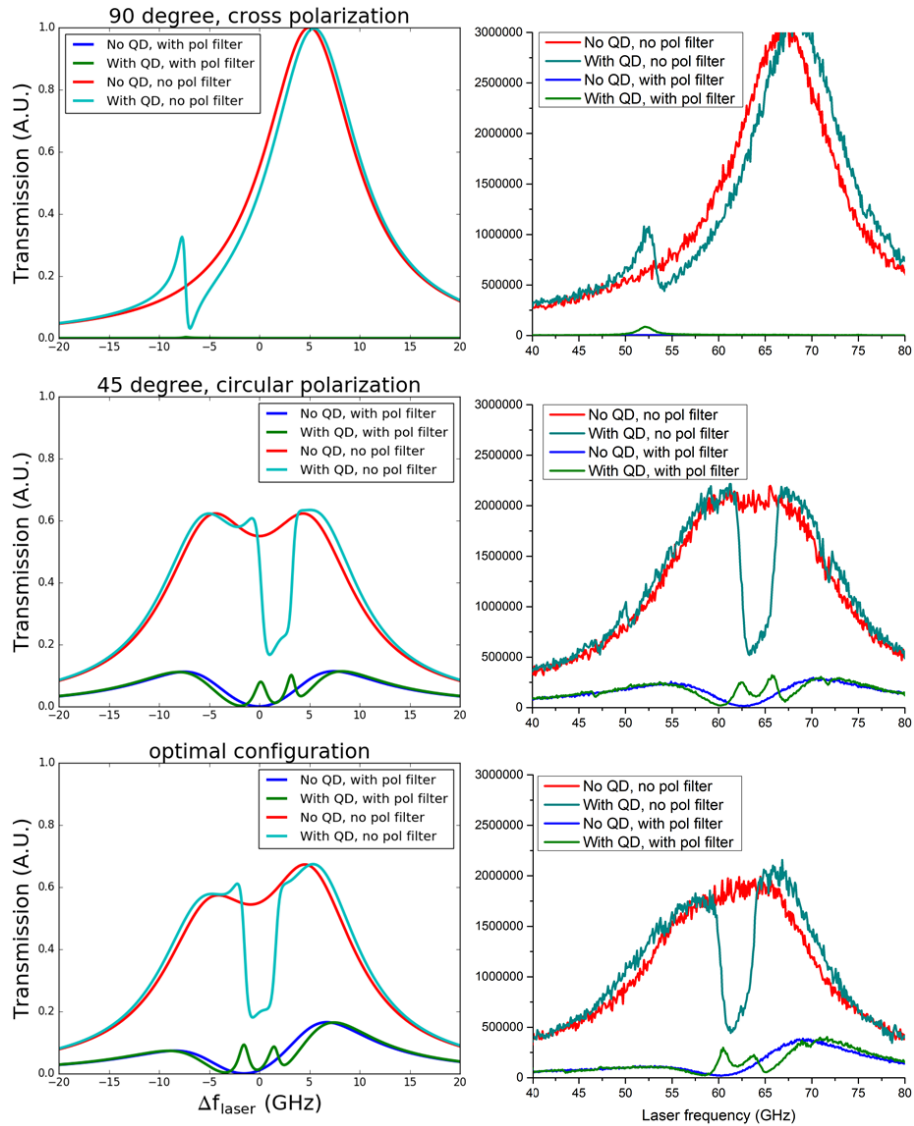


**Figure 4.3:** Simulated (left) and measured (right) transmitted intensity as a function of relative laser frequency for the three polarization configurations: 90Cross (top), 45Circ (center), and Optimal (bottom) at constant laser power. The transmission is shown with and without a quantum dot mode and with and without the output polarizer present. Figure 4.4 shows the intensity with the output polarizer present in more detail.

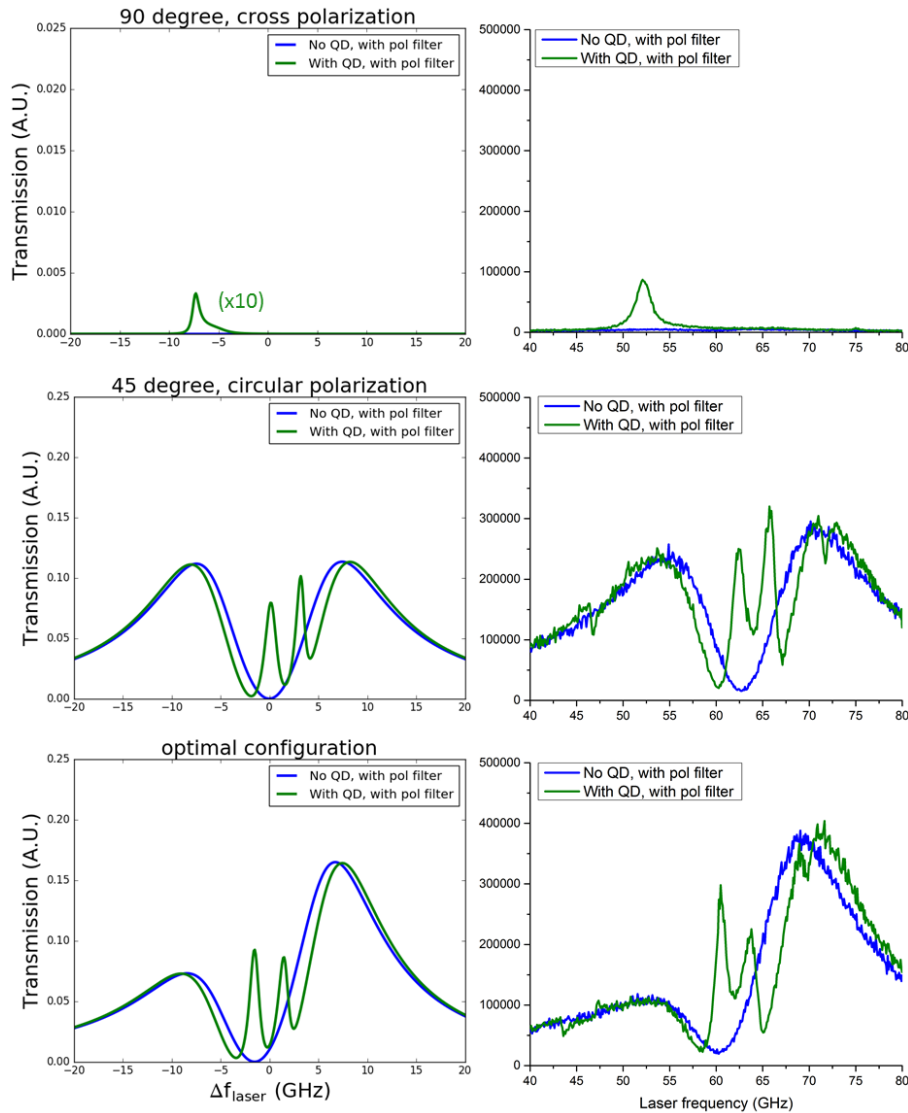


**Figure 4.4:** Simulated (left) and measured (right) transmitted intensity as a function of relative laser frequency with and without a quantum dot in the cavity for the three polarization configurations: 90Cross (top), 45Circ (center), and Optimal (bottom) at constant laser power. The measured intensity in the Optimal polarization configuration is about 3x the intensity in the 90 Cross configuration and 1.5x the intensity in the 45Circ configuration. The simulation predicts 10x less transmitted intensity for the 90Cross configuration than measured experimentally.

### 4.3 Single photon source quality

The simulation along with the experimental results tell us that, if we are indeed looking at single photons only in all three configurations, the brightness of the Optimal configuration is three times the intensity of the conventionally used 90Cross configuration (30x for the simulation) and that the 45Circ configuration is also already twice as bright (20x for the simulation). We do not yet know however if the intensity we see in the laser scans consists of single photons only. Therefore we will measure the intensity correlation function  $g^{(2)}(\tau)$  for different laser powers to analyze the quality of the single photon sources for the three different polarization configurations.

#### 4.3.1 Single photons and brightness

Although, as said, the intensity of the optimal configuration is three times as high as for the 90Cross configuration, we do not yet know if this intensity consists of single photons only. As stated briefly in methods, a  $g^{(2)}(\tau)$  (intensity correlation function) measurement allows us to find out if we are looking at single photons since a single photon source is characterized by anti-bunching. This anti-bunching shows up in the intensity correlation function as a dip at  $\tau = 0$  since a single photon cannot be detected by the two detectors at the same time (delay time between the detectors of 0). This behavior is purely quantum (since photons are inherently quantized) and cannot be explained classically.

For all three polarization configurations, the intensity correlation function shows a clear dip at  $\tau = 0$  up to 50% (figure 4.5), thus confirming that we are looking at single photons in all three configurations. In order to compare the single photon brightness of the three polarization configurations, however, we will measure  $g^{(2)}(\tau)$  for different excitation laser powers. This enables us to see the saturation of the quantum dot as a decrease of the dip at  $\tau = 0$ . The decrease of this dip should overlap for the three polarization configurations because it depends only on the quantum dot used and not on the polarization configuration.

This decrease of the dip (corresponding to an increase of  $g^{(2)}(0)$ ) does indeed overlap for the three polarization configurations as a function of excitation laser power (figure 4.6), thus confirming that we are indeed looking at the saturation of the quantum dot in all three configurations. For each  $g^{(2)}(\tau)$  measurement, however, the amount of single counts detected by the two APD's is recorded as well. When the height of the dip

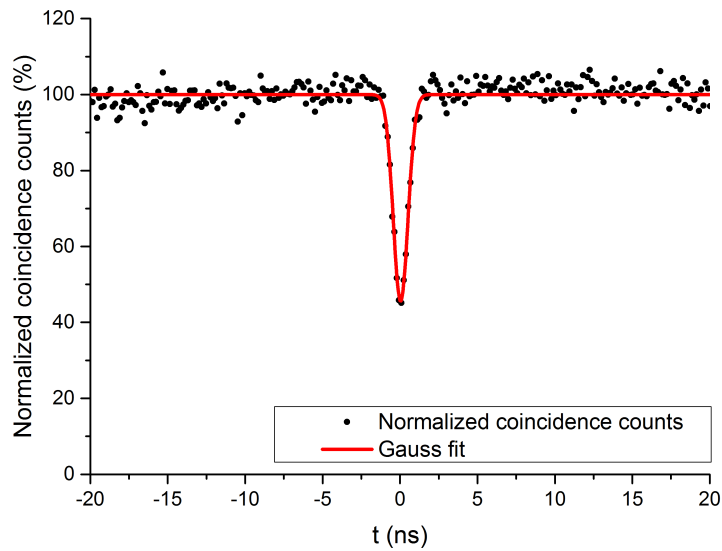


**Figure 4.5:** Measured photon correlation function  $g^{(2)}(\tau)$  (normalized to 100% for large  $\tau$ ) along with a Gauss fit at a laser power of 0.9nW with the polarization configuration set to Optimal. At  $\tau = 0$  the coincidence counts drop to 45% which corresponds to anti-bunching of photons.

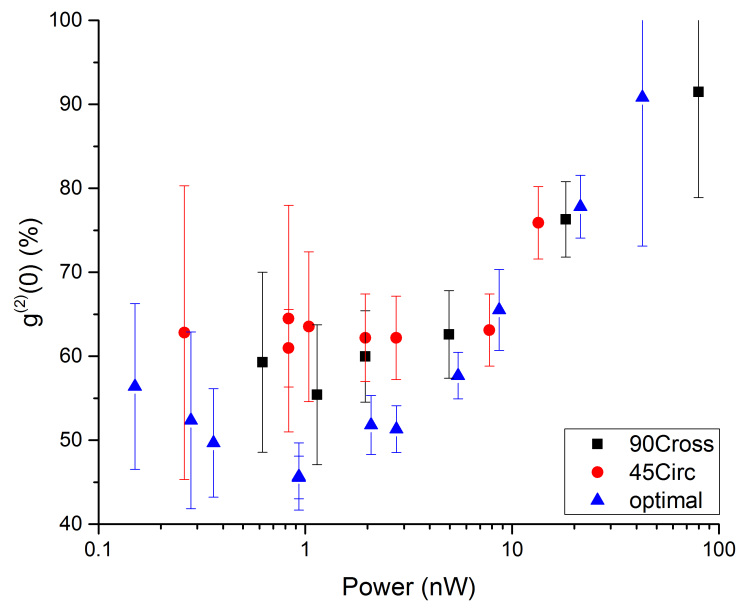


**Figure 4.6:** Fitted height of the dip in the measured intensity correlation function  $g^{(2)}(\tau)$  as a function of laser power for the three polarization configurations 90Cross, 45Circ, and Optimal. The dip height starts to diminish at a laser power of 5nW for all polarization configurations.

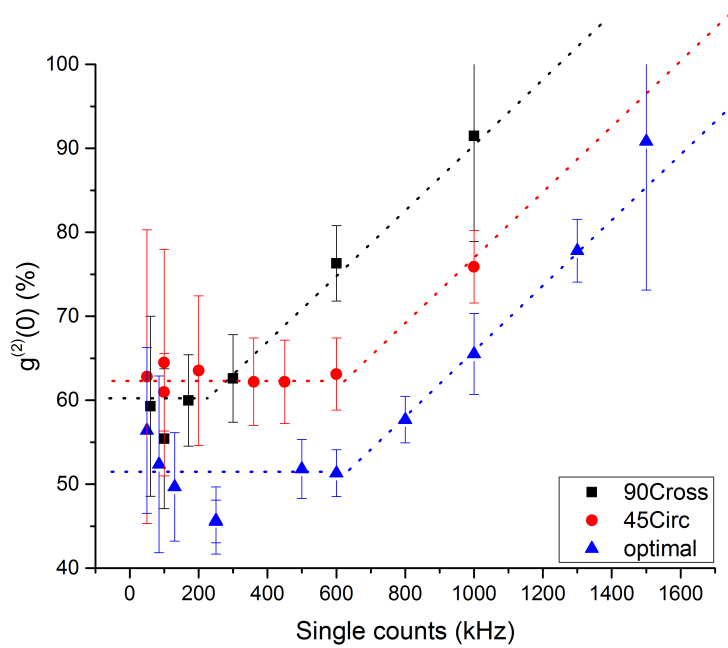


**Figure 4.7:** Fitted height of the dip in the measured intensity correlation function  $g^{(2)}(\tau)$  as a function of single counts for the three polarization configurations: 90Cross, 45Circ, and Optimal. The dashed parallel lines are added as a guide to the eye to show that the dip height starts to diminish at different count rates for the different polarization configurations.

is plotted as a function of single counts (figure 4.7), the points of the three polarization configurations do not overlap anymore: the dip starts to saturate at a different value of single counts for the three polarization configurations.

This difference in saturation of the quantum dot as a function of recorded single counts represents the relative brightness of the three different polarization configurations: the dip starts to saturate at higher counts for the optimal configuration than for the 90Cross and 45Circ configurations. Since the dip starts to saturate at the same laser power for all three configurations, this means that the optimal configuration yields a brighter single photon source. In order to compare the brightness of the three configurations, we can look at the recorded single counts as a function of excitation laser power.

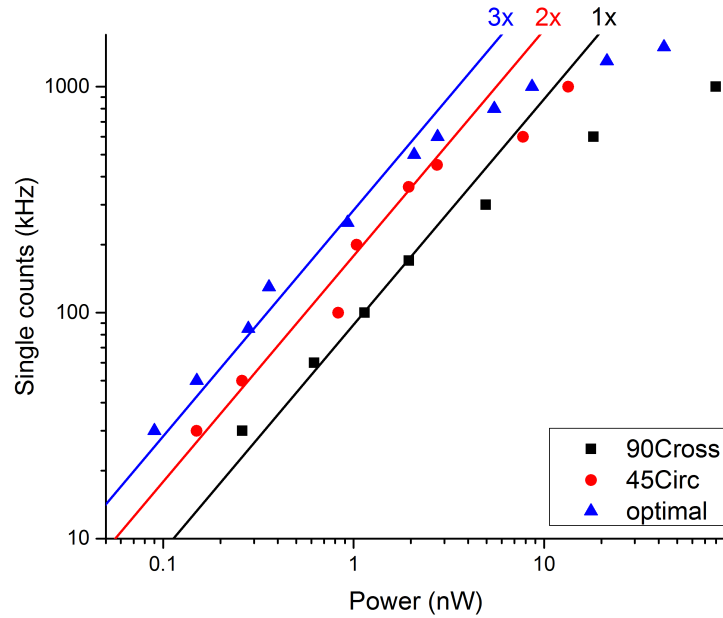


**Figure 4.8:** Single counts as a function of laser power for the three polarization configurations: 90Cross, 45Circ, and Optimal along with lines with a slope of 1x, 2x and 3x the fitted slope for the data points up to 2 nW of the 90Cross configuration.

### 4.3.2 Comparison

The 45Circ configuration generates twice the amount of single counts recorded in the 90Cross configuration where Optimal generates three times this amount (for the same laser power up to the saturation laser power of about 5 nW). This means that the optimal configuration yields a 3x brighter single photon source.

These factors of 2 and 3 found in the recorded single counts as a function of laser power (figure 4.8) correspond well with the factors between the height of the peaks in the measured laser scans (figure 4.4). Furthermore, the simulated laser scan line shapes closely match the measured laser scans (also including the factors between the height of the peaks). This means that the simulation can thus indeed help us to find the optimal polarization configuration for the brightest single photon source even though it is a semi-classical approximation and single photons are inherently quantum.

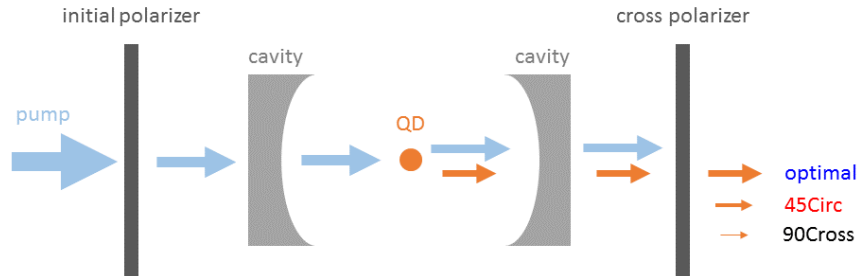


**Figure 4.9:** Schematic representation of the cavity with the quantum dot, the polarizers, and the pump (blue) and quantum dot (orange) light. Part of the light emitted by the quantum dot is filtered out by the cross polarizer, resulting in a lower transmitted intensity and coincidence count for the same excitation laser power. A brighter single photon source can be created by optimizing the polarization configuration to allow more light emitted by the quantum dot to pass through the cross polarizer while still blocking the laser light needed for excitation.

## 4.4 Mechanism behind brighter SPS

In a very simplified approach, we can understand the mechanism of how the brightness of a single photon source depends on the polarization configuration. Let us assume that the polarization of the incoming laser light does not influence the excitation rate of the quantum dot or the polarization of the light emitted by the quantum dot. The input polarizer sets the polarization of the light in the system (initial polarizer) and the output polarizer fully blocks this excitation light (cross polarizer). This blocking of the excitation light is the only constraint on the polarization configuration and the polarizers itself can be linear, circular, elliptical or a combination of those. Since no excitation laser light is transmitted in this system, all light that comes through the cross polarizer consists of single photons emitted by the quantum dot. A brighter single photon source can then be created by choosing a polarization configuration that allows more light emitted by the quantum dot to pass through the cross polarizer (figure 4.9).

With this oversimplified model we can also look at the results of the optimization of the polarization configuration as a function of quantum dot splitting and quantum dot angle. Recall that the polarization does not depend on these parameters (only on cavity splitting), but that the maximal transmitted intensity does. In our simple model, this means that the quantum dot angle is effectively rotating the polarization of the light

emitted by the quantum dot which changes the fraction of light that can pass through the cross polarizer (cf. figure 2.6, left to right). Note that a polarization degenerate quantum dot is unable to change the polarization of the light since it is essentially unpolarized. If the quantum dot had only one mode, however, it would be able to change the polarization (this is essentially an infinite quantum dot splitting).

A rotation of the quantum dot angle will thus change the amount of light that is transmitted by a static output polarizer, but the same oversimplified model works the other way around as well. As we have seen, the polarization configuration does depend on the cavity splitting. Thus, for a certain polarization of the light emitted by the quantum dot (determined mostly by the quantum dot angle), the amount of light that can pass through the cross polarizer depends on the polarization of this cross polarizer (cf. figure 2.7, top to bottom).

## 4.5 Discussion on the higher intensity

We have seen that the polarization configuration influences the brightness of the quantum dot single photon source and we can understand this behavior qualitatively with a simple model. Furthermore, the factor between the measured intensities of the peak of the laser scans matches with the factor of recorded single counts as a function of laser power for the different polarization configurations. This is as it should be since we recorded the counts at the peak frequency in the latter experiment. For the 90Cross configuration, however, the simulation predicts an intensity that is 10x as low as experimentally found. The question that remains to be answered is thus: where does this factor come from?

Part of the answer to this question is found from a voltage scan measurement. The voltage changes the excitation frequency of the quantum dot modes and is therefore used to, for example, tune the frequency of the quantum dot mode to the frequency of a cavity mode. For a 90Cross polarization configuration, a voltage scan produces lines that correspond with the quantum dot resonance frequency because the cavity modes are filtered out completely in this polarization configuration. However, in the voltage scan of the sample under study (figure 4.10), a peak appears for a voltage around 1.05 V which is three times as high as the other quantum dot mode lines. This peak is the quantum dot mode that we have been measuring in the 90Cross configuration precisely because it is so much brighter than the others. We have measured the same quantum dot mode in the other configurations, but as can be seen in the laser scan line shapes,

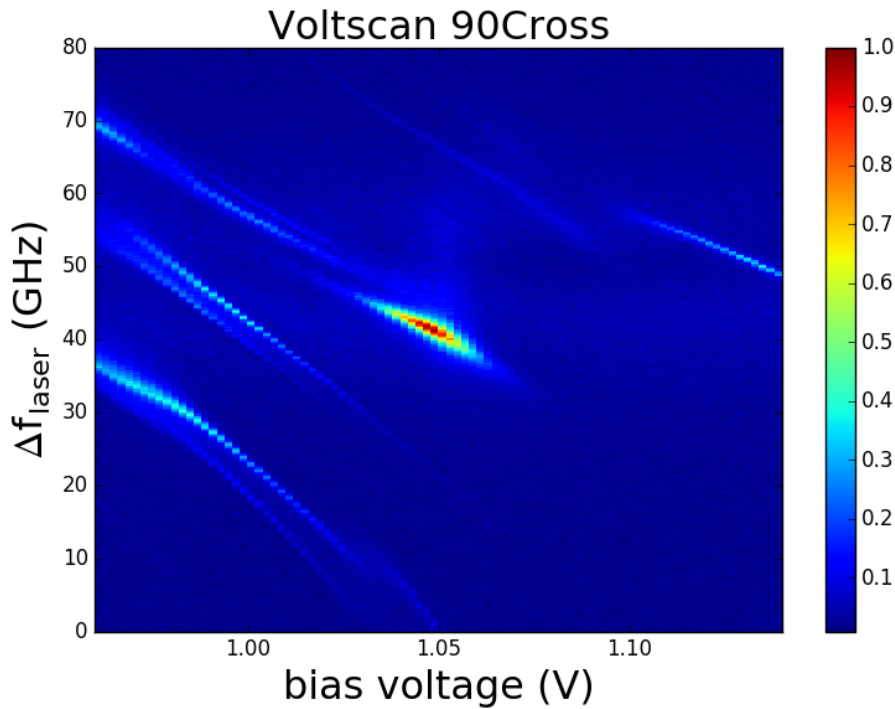


**Figure 4.10:** A measurement of the transmitted intensity in the 90Cross polarization configuration as a function of applied bias voltage to the PIN junction of the sample and relative laser frequency with a quantum dot in the cavity. The bright lines show that the bias voltage shifts the quantum dot transition energy by the quantum confined Stark effect. The transmitted intensity of the peak around 1.05 V is used for normalization and about 3x as large as the intensities of the other quantum dot lines.

the quantum dot was tuned to a higher frequency in those configurations. This frequency corresponds to a lower voltage of about 1.01 V and is thus not in the regime of the peak.

Although the peak is not 10x as high as the other quantum dot mode lines as predicted by the simulation, the peak is still significantly higher. Furthermore, the simulated intensity is very sensitive in the quantum dot angle around  $0^\circ$  and  $90^\circ$  in the 90Cross polarization configuration where it goes approximately as  $\sin^2\theta_{QD}$ , so the factor of 10 can be easily scaled down to a factor of 3 by slightly increasing the quantum dot angle (less than a degree). However, this remaining factor of 3 still has to be accounted for.

The proposed (hypothetical) mechanism for this increased intensity is therefore that an applied bias voltage around 1.05 V mediates a (phonon

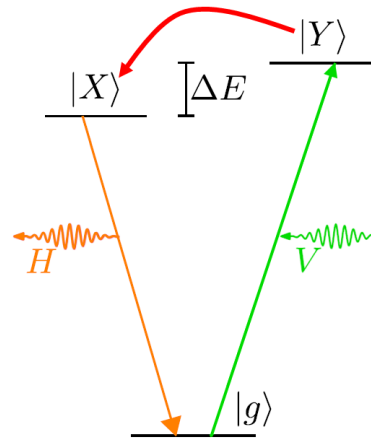


**Figure 4.11:** Proposed mechanism for the increased transmitted intensity in the 90° cross polarization configuration at a voltage of 1.05 V (figure 4.10). A vertically polarized photon excites the Y mode of the quantum dot (green arrow), the Y mode of the quantum dot relaxes to the X mode of the quantum dot (red arrow), and the X mode of the quantum dot emits a horizontally polarized photon. Figure adapted from Lodahl et al. [4].

assisted) relaxation from the Y to the X mode of the quantum dot (figure 4.11). If this is true, we can explain the increased intensity in the 90° cross configuration as follows. As we have seen, when the cavity frame and the quantum dot frame are at an angle to each other, the quantum dot can absorb light from the cavity mode filled with excitation laser light and emit a photon in either of the two cavity modes (figure 1.3). If the quantum dot angle is small, most light will be emitted in the cavity mode filled with the excitation laser light and will therefore not be transmitted by the cross polarizer.

However, if the light absorbed by the Y mode of the quantum dot can relax to the X mode with a certain probability, *vertically* polarized light will be absorbed by the Y mode of the quantum dot, this excited Y mode of the quantum dot will relax to the X mode of the quantum dot, and the X mode of the quantum dot will emit a *horizontally* polarized photon. This photon will pass through the cross polarizer since that polarizer is aligned with the empty cavity mode (i.e. the cavity mode without the excitation laser light).

This relaxation mechanism, however, has to have a longer lifetime than the mechanism where only one quantum dot mode is used. This lifetime of the quantum dot state can be extracted from the width of the dip in  $g^{(2)}(\tau)$ . Since the hopping mechanism is suspected to work only around

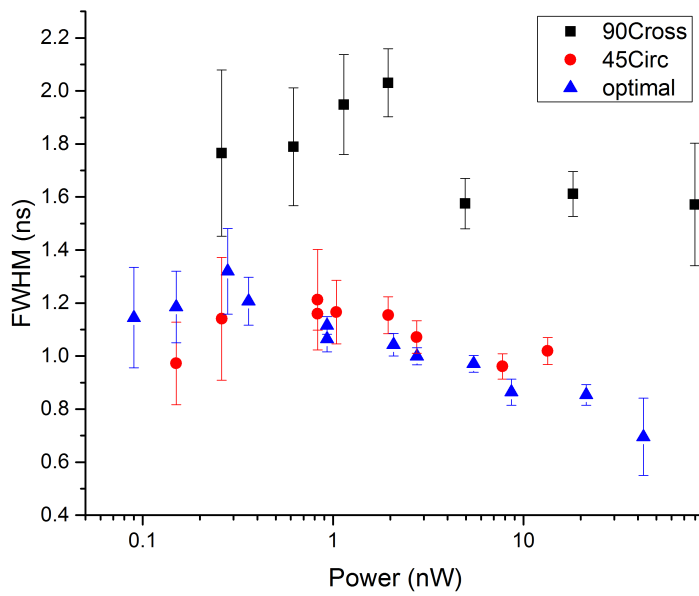


**Figure 4.12:** Fitted full width at half maximum of the dip in the measured intensity correlation function  $g^{(2)}(\tau)$  as a function of excitation laser power for the three polarization configurations 90Cross, 45Circ, and Optimal. The dip is wider in the 90Cross configuration which corresponds to a longer lifetime of the excited quantum dot state.

1.05 V bias voltage, it should only show up for the 90Cross configuration since the bias voltage for 45Circ and Optimal is around 1.01 V, well below the voltage of the peak. In order to check the quantum dot mode hopping hypothesis, we plotted the full width at half maximum as a function of recorded single counts (figure 4.12). The width of the dip in  $g^{(2)}(\tau)$  for the 90Cross configuration is about 1.7 ns while the width for the other two configurations is about 1.1 ns. This confirms that the lifetime of the quantum dot mode measured in the 90Cross configuration is indeed longer and thus that a relaxation mechanism between the Y mode and the X mode of the quantum dot could indeed be the reason for the increased intensity.

It is noteworthy to mention that correcting for the increased intensity of the quantum dot around 1.05 V would change the threefold increase in brightness for the optimal configuration into a tenfold increase over the brightness of the conventionally used polarization configuration. Although this is true, the quantum dot in the sample had a quantum dot angle quite close to  $90^\circ$  which is where the 90Cross configuration performs the absolute worst (since it goes as  $\sin(\theta_{QD})\cos(\theta_{QD})$ ). For quantum dot angles further away from  $\theta_{QD}=0^\circ$  or  $\theta_{QD}=90^\circ$ , the optimal configuration yields a single photon source that is about three times as bright as the conventional configuration. Therefore, we will stick with a threefold rather than a tenfold increase in brightness in this thesis.

## Conclusion

In this thesis we tried to increase the brightness of a cavity quantum electrodynamics single photon source by optimizing the polarization configuration of the input and output polarizer. We extended the conventional semi classical model of a single quantum dot in an optical cavity (formula 2.1) [20–23] to incorporate the double non-degeneracy of the quantum dot and the cavity (formula 2.2).

When we analyzed the results from the simulation based on this formula, we found that the conventionally used polarization configuration (90Cross) is not optimal for a bright single photon source. This is because the polarizations of the two cavity modes are orthogonal and the quantum dot is used to transfer light from one cavity mode to the other (figure 1.3). This transfer relies on the overlap between the polarization of the quantum dot with the polarizations of the cavity modes and therefore goes as  $\sin(\theta_{QD})\cos(\theta_{QD})$ . This is always less than the coupling from a cavity mode to the quantum dot and back to the same cavity mode which goes as  $\cos^2(\theta_{QD})$  (or  $\sin^2(\theta_{QD})$ ). Therefore, most of the emitted single photons are emitted back in the cavity mode polarization that is used to excite the quantum dot, but this light is blocked by the output polarizer.

In order to find a better (brighter) polarization configuration, we analyzed the effect the non-degenerate cavity modes have on the polarization of the light exiting the cavity and found that they make the cavity birefringent (figure 2.3). With this information we were able to find a more optimal polarization configuration (45Circ) that when tested in the lab indeed resulted in a single photon source that was twice as bright as the conventionally used configuration (90Circ).

When we knew that a brighter single photon source was thus possible, we let an optimization algorithm find the optimal polarization con-

figuration for a range of the three sample dependent parameters: cavity splitting, quantum dot splitting and quantum dot angle. This algorithm returned a polarization configuration consisting of an elliptical input polarization and a counter elliptical output polarization. This polarization configuration is nearly independent of the quantum dot splitting and the quantum dot angle and depends only in the circularity of the light on the cavity splitting (figures 2.4 and 2.5).

Based on these theoretical results we produced the optimal polarization configuration in the lab. We found that it returned an even brighter single photon source than the configuration found through analytical analysis of the simulation (45Circ) with a threefold increase in brightness over the conventionally used polarization configuration (90Cross)(figure 4.8).

All polarization configurations showed very similar single photon purity and saturation of the quantum dot (figure 4.6), thus confirming that the quality of the three polarization configurations (as separate single photon sources) was identical.

# Chapter 6

## Outlook

Although we have tested the optimization of the polarization configuration for only one sample, the single photon source quality was identical for the three different polarization configurations and the simulation correctly predicted the factor of increased brightness for each of these polarization configurations. Therefore, we assume that the simulation is correct for the whole range of sample dependent parameters (cavity splitting, quantum dot splitting and quantum dot angle). The sample dependent parameters from the sample that we tested are, however, far from optimal (cavity splitting 10 GHz, quantum dot splitting larger than 2 GHz, and quantum dot angle  $94^\circ$ ). We plan to fabricate a sample with optimal sample parameters (cavity splitting 5-15 GHz, quantum dot splitting larger than 1 GHz, and quantum dot angle  $20^\circ$ - $60^\circ$ ) which should result in a single photon source that can be three times as bright as the current one (figures 2.6 and 2.7). The most important sample dependent parameter to adjust is the quantum dot angle. To do so, we would need to change the axes of the cavity mode polarizations since the quantum dots are self-assembled and we cannot change the angle at which they grow easily. This will thus be our next step towards an even brighter single photon source.



## Acknowledgements

The work reported in this thesis could not have been done without the hard work of a lot of people. I would like to thank John Frey, Justin Norman, Henk Snijders, and Wolfgang Löffler for the development and fabrication of the samples. The theory and simulation presented in chapter 2 was a joint effort with David Kok. I would therefore especially like to thank David Kok for this collaboration on the theoretical development of the simulation but most importantly for his complementary (usually mathematical) insights and the fruitful discussions those insights often yielded.



# Bibliography

- [1] I. Aharonovich, D. Englund, and M. Toth, *Solid-state single-photon emitters*, Nat Photon **10**, 631 (2016), Review.
- [2] S. Buckley, K. Rivoire, and J. Vučković, *Engineered quantum dot single-photon sources*, Reports on Progress in Physics **75**, 126503 (2012).
- [3] J. L. O'Brien, A. Furusawa, and J. Vuckovic, *Photonic quantum technologies*, Nat Photon **3**, 687 (2009).
- [4] P. Lodahl, S. Mahmoodian, and S. Stobbe, *Interfacing single photons and single quantum dots with photonic nanostructures*, Rev. Mod. Phys. **87**, 347 (2015).
- [5] A. F. Koenderink, A. Alù, and A. Polman, *Nanophotonics: Shrinking light-based technology*, Science **348**, 516 (2015).
- [6] W. B. Gao, A. Imamoglu, H. Bernien, and R. Hanson, *Coherent manipulation, measurement and entanglement of individual solid-state spins using optical fields*, Nat Photon **9**, 363 (2015), Review.
- [7] T. E. Northup and R. Blatt, *Quantum information transfer using photons*, Nat Photon **8**, 356 (2014), Review.
- [8] V. Scarani, H. Bechmann-Pasquinucci, N. J. Cerf, M. Dušek, N. Lütkenhaus, and M. Peev, *The security of practical quantum key distribution*, Rev. Mod. Phys. **81**, 1301 (2009).
- [9] H.-K. Lo, M. Curty, and K. Tamaki, *Secure quantum key distribution*, Nat Photon **8**, 595 (2014), Review.

- 
- [10] S. Aaronson and A. Arkhipov, *The Computational Complexity of Linear Optics*, in *Proceedings of the Forty-third Annual ACM Symposium on Theory of Computing, STOC '11*, pages 333–342, New York, NY, USA, 2011, ACM.
- [11] Somaschi N., Giesz V., D. Santis L., L. C., A. P., Hornecker G., P. L., Grange T., Antón C., Demory J., Gómez C., Sagnes I., L.-K. D., Lemaître A., Auffeves A., W. G., Lanco L., and Senellart P., *Near-optimal single-photon sources in the solid state*, *Nat Photon* **10**, 340 (2016), Article.
- [12] X. Ding, Y. He, Z.-C. Duan, N. Gregersen, M.-C. Chen, S. Unsleber, S. Maier, C. Schneider, M. Kamp, S. Höfling, C.-Y. Lu, and J.-W. Pan, *On-Demand Single Photons with High Extraction Efficiency and Near-Unity Indistinguishability from a Resonantly Driven Quantum Dot in a Micropillar*, *Phys. Rev. Lett.* **116**, 020401 (2016).
- [13] J.-H. Kim, T. Cai, C. J. K. Richardson, R. P. Leavitt, and E. Waks, *Two-photon interference from a bright single-photon source at telecom wavelengths*, *Optica* **3**, 577 (2016).
- [14] H. Wang, Z.-C. Duan, Y.-H. Li, S. Chen, J.-P. Li, Y.-M. He, M.-C. Chen, Y. He, X. Ding, C.-Z. Peng, C. Schneider, M. Kamp, S. Höfling, C.-Y. Lu, and J.-W. Pan, *Near-Transform-Limited Single Photons from an Efficient Solid-State Quantum Emitter*, *Phys. Rev. Lett.* **116**, 213601 (2016).
- [15] J. C. Loredó, N. A. Zakaria, N. Somaschi, C. Anton, L. de Santis, V. Giesz, T. Grange, M. A. Broome, O. Gazzano, G. Coppola, I. Sagnes, A. Lemaître, A. Auffeves, P. Senellart, M. P. Almeida, and A. G. White, *Scalable performance in solid-state single-photon sources*, *Optica* **3**, 433 (2016).
- [16] C. Dory, K. A. Fischer, K. Müller, K. G. Lagoudakis, T. Sarmiento, A. Rundquist, J. L. Zhang, Y. Kelaita, and J. Vučković, *Complete Coherent Control of a Quantum Dot Strongly Coupled to a Nanocavity*, *Sci Rep* **6**, 25172 (2016), 27112420[pmid].
- [17] S. Sun, H. Kim, G. S. Solomon, and E. Waks, *A quantum phase switch between a single solid-state spin and a photon*, *Nat Nano* **11**, 539 (2016), Article.
- [18] C. Santori, M. Pelton, G. Solomon, Y. Dale, and Y. Yamamoto, *Triggered Single Photons from a Quantum Dot*, *Phys. Rev. Lett.* **86**, 1502 (2001).

- 
- [19] S. Strauf, N. G. Stoltz, M. T. Rakher, L. A. Coldren, P. M. Petroff, and D. Bouwmeester, *High-frequency single-photon source with polarization control*, *Nat Photon* **1**, 704 (2007).
- [20] M. Bakker, *Cavity quantum electrodynamics with quantum dots in micro-cavities*, publisher not identified, Netherlands, 2015.
- [21] A. Auffèves-Garnier, C. Simon, J.-M. Gérard, and J.-P. Poizat, *Giant optical nonlinearity induced by a single two-level system interacting with a cavity in the Purcell regime*, *Phys. Rev. A* **75**, 053823 (2007).
- [22] V. Loo, C. Arnold, O. Gazzano, A. Lemaître, I. Sagnes, O. Krebs, P. Voisin, P. Senellart, and L. Lanco, *Optical Nonlinearity for Few-Photon Pulses on a Quantum Dot-Pillar Cavity Device*, *Phys. Rev. Lett.* **109**, 166806 (2012).
- [23] E. Waks and J. Vuckovic, *Dipole Induced Transparency in Drop-Filter Cavity-Waveguide Systems*, *Phys. Rev. Lett.* **96**, 153601 (2006).
- [24] M. A. Armen and H. Mabuchi, *Low-lying bifurcations in cavity quantum electrodynamics*, *Phys. Rev. A* **73**, 063801 (2006).
- [25] H. Snijders, J. A. Frey, J. Norman, M. P. Bakker, E. C. Langman, A. Gossard, J. E. Bowers, M. P. van Exter, D. Bouwmeester, and W. Löffler, *Purification of a single-photon nonlinearity*, *Nature Communications* **7**, 12578 EP (2016), Article.